

**THE EFFECT OF ERISTOSTATIN ON MELANOMA-NATURAL KILLER
CELL INTERACTIONS**

by

Stefan M. Hailey

A thesis submitted to the Faculty of the University of Delaware in partial fulfillment of
the requirements for the degree of Master of Science in Biological Sciences

Fall 2011

Copyright 2011 Stefan M. Hailey
All Rights Reserved

**THE EFFECT OF ERISTOSTATIN ON MELANOMA-NATURAL KILLER
CELL INTERACTIONS**

by

Stefan M. Hailey

Approved: _____
Mary Ann McLane, Ph.D., MLS (ASCP)
Professor in charge of thesis on behalf of the Advisory Committee

Approved: _____
Randall L. Duncan, Ph.D.
Chair of the Department of Biological Sciences

Approved: _____
George H. Watson, Ph.D.
Dean of the College of Arts and Sciences

Approved: _____
Charles G. Riordan, Ph.D.
Vice Provost for Graduate and Professional Education

ACKNOWLEDGMENTS

I would like to give my appreciation to my advisor, Dr. Mary Ann McLane, for allowing me to work on such a great research project. Over, the past two years, her guidance and encouragement has helped me develop my skills as a research scientist.

I would also like to give thanks to my thesis committee members: Dr. Ulhas Naik, Dr. Gary Laverty for their advice and input in this process and Dr. Elizabeth Adams for all her help and patience in teaching me Atomic Force Microscopy. In addition to my committee members, I thank all the members of the McLane lab past and present for laying the ground work of my project.

Finally, I would like to say thank you to my friends and family for their support during this endeavor; without them this accomplishment would not be possible.

TABLE OF CONTENTS

| | |
|-----------------------------|------------|
| LIST OF TABLES..... | vi |
| LIST OF FIGURES..... | vii |
| ABSTRACT | x |

Chapter

| | |
|--|-----------|
| 1 INTRODUCTION | 1 |
| 1.1 Melanoma | 1 |
| 1.2 Integrins and RGD Motifs | 2 |
| 1.3 Natural Killer Cells..... | 3 |
| 1.4 Disintegrins and Eristostatin..... | 5 |
| 1.5 Atomic Force Microscopy | 7 |
| 2 MATERIALS AND METHODS..... | 10 |
| 2.1 Materials | 10 |
| 2.2 Cell Culture | 11 |
| 2.3 Natural Killer Cell Isolation | 11 |
| 2.4 Preparation of Recombinant Eristostatin..... | 12 |
| 2.5 Platelet Aggregation | 13 |
| 2.6 Atomic Force Microscopy | 13 |
| 2.7 Flow Cytometry | 14 |
| 2.8 Statistical Analysis | 16 |
| 3 RESULTS..... | 17 |
| 3.1 Platelet Aggregation | 17 |
| 3.2 Direct unbinding of eristostatin and human melanoma cells | 17 |
| 3.3 Partial inhibition of the eristostatin-melanoma cell interaction with RGDS peptide..... | 21 |
| 3.4 Purity of freshly isolated natural killer cells..... | 32 |
| 3.5 Effect of eristostatin on natural killer cell-melanoma cell interactions..... | 32 |
| 3.6 Surface expression of NKG2D ligand MICA/B | 41 |

| | |
|--|-----------|
| 4 DISCUSSION AND CONCLUSIONS..... | 45 |
| 4.1 Discussion..... | 45 |
| 4.2 Conclusion..... | 60 |
| REFERENCES | 63 |
| Appendix | 74 |
| PERMISSION LETTER..... | 75 |

LIST OF TABLES

| | | |
|-----------|--|----|
| Table 3.1 | Percentage of total contacts which showed unbinding events in the presence or absence of 500 nM erlotinib in solution with Er on the AFM tip | 20 |
| Table 3.2 | Percentage of total contacts which showed unbinding events in the presence or absence of 200 μ M RGDS peptide in solution with Er on the AFM tip | 27 |
| Table 3.3 | Summary comparison of AFM unbinding populations between erlotinib functionalized tips and melanoma cells | 31 |
| Table 3.4 | Summary comparison of AFM unbinding populations between natural killer cell functionalized tips and melanoma cells | 40 |
| Table 4.1 | Integrin surface expression repertoire on six human melanoma cell lines using flow cytometry versus literature | 50 |

LIST OF FIGURES

| | | |
|------------|--|----|
| Figure 3.1 | Representative platelet aggregation assay using eristostatin batch 7.2 208.081 | 18 |
| Figure 3.2 | Average unbinding force between melanoma cells and eristostatin on the AFM cantilever tip..... | 19 |
| Figure 3.3 | Frequency of unbinding events between C8161 and eristostatin functionalized AFM cantilever tips in the presence or absence of 500 nM eristostatin of at least 3 experiments | 22 |
| Figure 3.4 | Frequency of unbinding events between MV3 and eristostatin functionalized AFM cantilever tips in the presence or absence of 500 nM eristostatin of at least 3 experiments..... | 22 |
| Figure 3.5 | Frequency of unbinding events between M24met and eristostatin functionalized AFM cantilever tips in the presence or absence of 500 nM eristostatin of at least 3 experiments..... | 23 |
| Figure 3.6 | Frequency of unbinding events between 1205Lu and eristostatin functionalized AFM cantilever tips in the presence or absence of 500 nM eristostatin of at least 3 experiments | 23 |
| Figure 3.7 | Frequency of unbinding events between WM164 and eristostatin functionalized AFM cantilever tips in the presence or absence of 500 nM eristostatin of at least 3 experiments | 24 |
| Figure 3.8 | Frequency of unbinding events between SBcl2 and eristostatin functionalized AFM cantilever tips in the presence or absence of 500 nM eristostatin of at least 3 experiments | 24 |
| Figure 3.9 | Average unbinding force between melanoma cells and eristostatin on the AFM cantilever tip..... | 26 |

| | | |
|-------------|---|----|
| Figure 3.10 | Frequency of unbinding events between C8161 and eristostatin functionalized AFM cantilever tips in the presence or absence of 200 μ M RGDS peptide of at least 3 experiments | 28 |
| Figure 3.11 | Frequency of unbinding events between MV3 and eristostatin functionalized AFM cantilever tips in the presence or absence of 200 μ M RGDS peptide of at least 3 experiments | 28 |
| Figure 3.12 | Frequency of unbinding events between M24met and eristostatin functionalized AFM cantilever tips in the presence or absence of 200 μ M RGDS peptide of at least 3 experiments | 29 |
| Figure 3.13 | Frequency of unbinding events between 1205Lu and eristostatin functionalized AFM cantilever tips in the presence or absence of 200 μ M RGDS peptide of 1 experiments | 29 |
| Figure 3.14 | Frequency of unbinding events between WM164 and eristostatin functionalized AFM cantilever tips in the presence or absence of 200 μ M RGDS peptide of at least 3 experiments | 30 |
| Figure 3.15 | Frequency of unbinding events between SBcl2 and eristostatin functionalized AFM cantilever tips in the presence or absence of 200 μ M RGDS peptide of at least 3 experiments | 30 |
| Figure 3.16 | Representative flow cytometry histogram of freshly isolated natural killer cells | 33 |
| Figure 3.17 | Natural killer cell (arrow) attached to tip of AFM cantilever tip engaged on WM164 human melanoma cell (200x)..... | 34 |
| Figure 3.18 | Average unbinding force between melanoma cells and natural killer cell on the AFM cantilever tip | 35 |
| Figure 3.19 | Frequency of unbinding events between C8161 and natural killer cell functionalized AFM cantilever tips in the presence or absence of 500 nM eristostatin of at least 3 experiments..... | 37 |
| Figure 3.20 | Frequency of unbinding events between MV3 and natural killer cell functionalized AFM cantilever tips in the presence or absence of 500 nM eristostatin of at least 3 experiments..... | 37 |

| | | |
|-------------|---|----|
| Figure 3.21 | Frequency of unbinding events between M24met and natural killer cell functionalized AFM cantilever tips in the presence or absence of 500 nM eristostatin of at least 3 experiments..... | 38 |
| Figure 3.22 | Frequency of unbinding events between 1205Lu and natural killer cell functionalized AFM cantilever tips in the presence or absence of 500 nM eristostatin of at least 3 experiments..... | 38 |
| Figure 3.23 | Frequency of unbinding events between WM164 and natural killer cell functionalized AFM cantilever tips in the presence or absence of 500 nM eristostatin of at least 3 experiments..... | 39 |
| Figure 3.24 | Frequency of unbinding events between SBcl2 and natural killer cell functionalized AFM cantilever tips in the presence or absence of 500 nM eristostatin of at least 3 experiments..... | 39 |
| Figure 3.25 | MICA/B expression on the surface of C8161 human melanoma cells..... | 41 |
| Figure 3.26 | MICA/B expression on the surface of MV3 human melanoma cells..... | 42 |
| Figure 3.27 | MICA/B expression on the surface of M24met human melanoma cells..... | 42 |
| Figure 3.28 | MICA/B expression on the surface of WM164 human melanoma cells..... | 43 |
| Figure 3.29 | MICA/B expression on the surface of SBcl2 human melanoma cells..... | 43 |
| Figure 3.30 | MICA/B expression on the surface of 1205Lu human melanoma cells..... | 44 |
| Figure 4.1 | Confocal images of melanoma cell line 1205Lu stained with FITC-labeled eristostatin (A) in the presence of soluble eristostatin at 69 nM (B), 139 nM (C), 500 nM (D), and 1000 nM (E) concentrations..... | 47 |
| Figure 4.2 | Natural killer cell integrin-mediated intracellular signaling and cytotoxicity | 57 |

ABSTRACT

Malignant melanoma is difficult to treat due to its resistance to chemotherapeutic regimens. Discovery of new pharmaceuticals with inhibitory potential can be helpful in the development of novel treatments. The purified snake venom disintegrin eristostatin, from the viper *Eristocophis macmahoni*, caused immunodeficient mice to be significantly protected (47-57%, $p < 0.003$) from development of lung colonization when melanoma cells and the disintegrin were co-injected *in vivo* into the lateral tail vein compared to vehicle controls. Cytotoxicity assays suggested that eristostatin makes the melanoma cells a better target for lysis by human natural killer cells, while previous investigators have demonstrated that melanoma cells may alter NKG2D ligand expression in order to escape natural killer cell targeting. Direct binding assays using atomic force microscopy show eristostatin does bind the surface of the six melanoma cell lines tested and this interaction is specific. Eristostatin binding was partially inhibited by the addition of 0.2 mM soluble RGDS peptide suggesting an integrin as one likely, but not the sole, binding partner. Studies were done with melanoma cells on a culture dish and natural killer cells attached to the AFM cantilever tip, in the presence and absence of 0.5 μ M eristostatin. There were four major populations of interactions which, interestingly, showed altered

frequency and unbinding strength in the presence of eristostatin. Surface expression assays showed that eristostatin did not cause a change in the surface expression of the NKG2D ligand, MICA/B.

Chapter 1

INTRODUCTION

1.1. Melanoma

Malignant melanoma incidence rates have consistently increased over the past 35 years affecting men and women of all ages and ethnicities. It is estimated that in 2010 approximately 68,000 people were diagnosed with melanoma and almost 8,700 cases were fatal (Altekruse *et al.*, 2009). Currently, the estimated lifetime risk of developing melanoma is 1 in 58 and this is expected to reach 1 in 50 by 2015 (Rigel *et al.*, 2010). With growing occurrence it is of utmost importance to discover novel strategies for melanoma therapies.

Melanoma in the primary stage has a 5 year survival rate of 98% which decreases to 15.9% after metastasis (Altekruse *et al.*, 2009). Melanoma metastasis involves the spread of cancer cells from a primary site to other areas. The initial development of metastatic melanoma is defined by four pre-malignant steps: common nevus, dysplastic nevi, radial growth phase, and vertical growth phase (Hsu *et al.*, 2002). The initial step is characterized by a common nevus which forms a coalescent nest of nevocytes that display aberrant cellular growth. The second stage in melanoma progression is the formation of dysplastic nevi which show an increase in cytological

and architectural atypia compared to normal melanocytes. Radial growth phase (RGP) primary melanoma is locally invasive but does not show rapid growth and is still confined within the epidermis. Vertical growth phase (VGP) is characterized by invasion into the dermis and subcutaneous tissue. Melanoma progression culminates in metastasis and the migration of cancerous cells from the primary tissue to a secondary site. This process is influenced by both genetic factors and the tissue microenvironment (Hsu *et al.*, 2002; Herlyn *et al.*, 1987).

1.2. Integrins and RGD motifs

Integrins make up a large family of cell surface receptors. Structurally, they are heterodimeric glycoproteins composed of alpha (α) and beta (β) transmembrane subunits (Liddington, 2003). There are 24 unique integrins which form from the pairing of 18 α and 8 β subunits. Though different integrins may bind the same ligand, each of these 24 integrins is thought to have specific functions distinct from one another (Hynes, 2002; Humphries *et al.*, 2006). Integrins, as their name implies, integrate the extracellular matrix (ECM) with the intracellular cytoskeleton and are responsible for cell-ECM and cell-cell adhesions. Through this intimate relationship, integrins allow the cell to respond to changes in the extracellular environment by modulating many characteristics of cellular behavior: proliferation, survival, shape, motility, and differentiation (Hynes, 2002; Giancotti and Ruoslahti, 1999). Due to this critical function as governors of cellular behavior, they play a large role in the

initiation, progression, and metastasis of cancerous tissues and can thus be important targets for anti-cancer therapies (Desgrosellier and Cheresh, 2010).

Many of the ligands with which integrins bind contain short amino acid sequences that are essential for recognition. One such sequence is Arginine-Glycine-Aspartic acid (RGD). The RGD tripeptide was initially identified as the cell-attachment domain of fibronectin but is now known to serve as a recognition motif of multiple ligands for various integrins. Though the RGD sequence is important in recognition specificity, flanking residues, tertiary structure, and differences in the integrin binding pockets can alter the interactions between ligand and integrin (Ruoslahti and Pierschbacher, 1987; Plow *et al.*, 2000). All five α_v integrins, two β_1 integrins, and $\alpha_{IIb}\beta_3$ are recognized as containing the active binding site, at which the RGD sequence binds at an interface between the α and β subunits. This spatial arrangement allows the arginine to fit into a cleft in the β -propeller motif of the α subunit and the aspartic acid to coordinate a cation which associates in the von Willebrand factor A-domain of the β subunit. Despite this specificity, RGD binding integrins are among the most promiscuous and can bind several ECM and non-ECM ligands with variable affinities (Humphries *et al.*, 2006).

1.3. Natural Killer Cells

Natural Killer (NK) cells are large granular lymphocytes which are principally responsible for the innate immune response in mammals. They have three major functional characteristics: cytotoxicity, cytokine and chemokine secretion, and contact-

dependent cell costimulation. Their cytotoxic ability is derived from the secretion of cytolytic lysosomes containing perforin and granzymes which are largely effective in the killing of tumorigenic and virally infected cells. NK cells also secrete a number of cytokines and chemokines which can affect NK function by increasing proliferation or varying cytotoxicity by altering activation. Contact-dependent cell costimulation allows NK cells, through the expression of costimulatory molecules, to signal other immune cells such as T and B cells to the location of infection or cellular stress. The cytotoxicity of NK cells is dependent on a balance between activation and inhibitory signals. A shift in this balance due to changes in activating receptors such as NKG2D, its ligand, MHC-class I chain-related protein A or B (MICA and MICB), or inhibitory receptors which recognize MHC-class I, can alter NK cytotoxicity (Zimmer, 2010). It is important to note that some melanomas, including cell lines and freshly isolated metastases, do not express MICA on their surface but retain immature forms of the NKG2D ligand within their endoplasmic reticulum (ER) which provides an advantage against NK cytotoxicity. The surface expression of MICA on melanoma cells varies largely between cells dependent on stage and the location from which the tissue was isolated. In addition, levels of MICA surface expression do not directly correlate with cytotoxicity; however, the percentage of cytotoxicity which occurs can be positively correlated with the ratio of NKG2D ligands, the activating signal for NK cell mediated lysis, to the inhibitory signal, MHC class I expression (Fuentes *et al.*, 2008).

1.4. Disintegrins and Eristostatin

Disintegrins are a family of proteins which have low molecular weights (41-84 amino acids), are cysteine-rich, and exist as monomers and dimers (McLane *et al.*, 1998; McLane *et al.*, 2008). They are isolated from the venom of various viper snakes and were originally only defined as potent inhibitors of platelet aggregation through binding of the fibrinogen receptor, $\alpha_{IIb}\beta_3$ (Gould *et al.*, 1990; Ouyang *et al.*, 1983). It is thought that disintegrins form via a proteolytic pathway from precursors of the PII class of snake venom metalloproteinases or are coded by short-coding mRNAs (Calvete *et al.*, 2005; Okuda *et al.*, 2002).

Within most disintegrins, a binding motif is arranged in an RGD loop which mimics the adhesive properties of peptide motifs present in molecules such as fibronectin, fibrinogen, vitronectin, and VCAM-1 (McLane *et al.*, 2004). This adhesive loop is maintained in the correct conformation by the formation of disulfide bridges. These conserved S-S linkages cause proteins within this family to be highly homologous. Monomeric disintegrins are generally classified into three groups based on amino acid length and their cysteine content. Short disintegrins are composed of 41-51 amino acids and contain 8 cysteines (accutin, echistatin, eristocophin, eristostatin, etc.). Disintegrins of approximately 70 amino acids and 12 cysteines are considered medium length (albolabrin, kistrin, trigramin, flavoridin, etc.). Large disintegrins such as bitistatin contain 84 amino acids and 14 cysteines. However, slight variations in their structure including the addition of cysteine motifs in the C-

terminus or disulfide bridges allow significant differences in integrin binding and affinity (McLane *et al.*, 2008)

Eristostatin (Er) is a short monomeric disintegrin isolated from the venom of *Eristicophis macmahoni* and contains 49 residues which include an RGD loop formed by 2 of its 4 disulfide linkages. In 1994, McLane *et al.* reported Er to be a potent inhibitor of adenosine diphosphate (ADP)-induced platelet aggregation. Eristostatin (25µg/ml) also caused a significant inhibition of lung and liver metastases due to B16F1 murine melanoma cells in an experimental metastasis model using C57BL/6 mice (Beviglia *et al.*, 1995; Morris *et al.*, 1995). In addition to these studies, Danen *et al.* (1998) observed that eristostatin inhibited lung colonization by human melanoma in an experimental murine metastasis model. Lung metastases were inhibited by 67% ($p = 0.0007$), 55% ($p = 0.008$), and 50% ($p = <0.0001$) due to eristostatin following an intravenous injection of MV3, M24met, and C8161 human melanoma cells, respectively, into nude mice deficient in T and B cells but not deficient in natural killer cells (Danen *et al.*, 1998; McLane *et al.*, 2003). The reduction in lung colonization was thought to be mediated in part by the interference in binding of integrin $\alpha_4\beta_1$ to VCAM (Danen *et al.*, 1998). Eristostatin significantly hindered the migration on fibronectin of five melanoma cell lines in a concentration-dependent manner, while not having an effect on proliferation or angiogenesis. In a set of function-blocking experiments using antibodies for both anti- α_v and anti- β_1 there was substantial heterogeneity among the five cell lines in their ability to adhere to eristostatin-coated

plates. Additionally, MV3 and M24met melanoma cell lines showed decreased adhesion to fibronectin-coated plates and MV3 did not express the β_3 subunit which is part of the major group of RGD-dependent integrins. This evidence may indicate that eristostatin may also act through a non-RGD dependent mechanism (Tian *et al.*, 2007).

Exploring eristostatin's mode of action in the inhibition of metastases, McLane *et al.* (2001) showed that the cytotoxic effect of NK-like TALL-104 (O'Connor *et al.*, 1991; Cesano and Santoli, 1992) cells increased when eristostatin was added to SBcl2 melanoma cells and/or the TALL-104 cells. However, the mechanism by which eristostatin acts on murine and human melanoma cells is still unknown. In an effort to elucidate the functional residues of eristostatin, a series of alanine mutations were performed. Residues within the RGD-loop and within the C-terminus were determined to be critical for eristostatin function (Tian *et al.*, 2007).

1.5. Atomic Force Microscopy

In the last decade major improvements have been made in techniques designed to measure cell-cell, cell-matrix, and receptor-ligand interactions. These interactions are dependent largely on adhesion molecules such as integrins and play a large role in many cell functions such as cell communication, migration and tumor metastasis (Desgrosellier and Cheresch, 2010). Atomic force microscopy (AFM) belongs to a broad group of instruments called scanning probe microscopes used to image and characterize the properties of material, chemical, and biological surfaces at the atomic scale and in three dimensions, x, y, and z (Blanchard, 1996).

A common AFM technique used to measure the strength of interactions between a sample and the AFM tip is called force spectroscopy. This technique requires the tip to approach the sample surface and then be retracted while cantilever deflections are detected via a photodiode that recognizes the changes in voltage from a laser reflected off the back of the cantilever. Tips may be functionalized with specific chemical or biological species in order to study specific interactions. This interaction is commonly expressed as unbinding force (nN) and is directly related to the characteristics of the cantilever by Hooke's law:

$$F = k\alpha V \quad [1]$$

in which k is the spring constant (resonance frequency) of the cantilever, α is the cantilever deflection sensitivity (rigidity), and V is the cantilever deflection in volts. Through this relationship, AFM allows for the direct quantitative measurement of attractive and repulsive forces at the molecular level (Han and Serry, 2008; Benoit and Gaub, 2002).

AFM force spectroscopy was used for the first time to characterize the specific interaction forces on intact mammalian cells by Lehenkari et al. (1999). In an effort to detect interactions between individual molecules, the unbinding forces between an individual integrin, $\alpha_v\beta_3$, on osteoclasts and several isolated proteins such as anti- $\alpha_v\beta_3$ monoclonal antibody F11, synthetic RGD peptides, and the disintegrin, echistatin, were determined (Lehenkari and Horton, 1999). Advancing AFM's applications further, Puech et al. (2006) used AFM to determine the unbinding forces in the pico

Newton (pN) range of cell-cell and cell-ECM adhesive forces between a cantilever functionalized with WM115 melanoma cells and human umbilical vein endothelial cells or a fibronectin coated surface respectively. Zhang et al. (2004) proved AFM to be a valuable tool in studying leukocyte-endothelial interactions. By functionalizing the AFM tip with a promyelocytic leukemia cell and measuring the changes in force after the addition of different antibodies and peptides, they were able to demonstrate the importance of β_1 -integrins and $\alpha_v\beta_3$ in leukocyte-endothelial cell adhesion and transmigration.

Therefore, the hypothesis for this project was that eristostatin will bind the surface of each melanoma cell causing changes in the interactions between the melanoma cell and natural killer cell. To test this hypothesis, force spectroscopy using the atomic force microscope, confirmed that eristostatin binds each melanoma cell line's surface and characterized the unbinding interactions, specifically determining if those interactions were RGD-dependent. In addition, the effect of eristostatin on the unbinding characteristics of the melanoma cell-natural killer cell interactions were examined. Finally, using cytometric analysis, changes in the surface expression of the NK killing receptor ligand, MICA, in the presence and absence of eristostatin were identified.

Chapter 2

METHODS AND MATERIALS

2.1. Materials

Human melanoma cell lines 1205Lu (metastatic), WM164 (vertical growth phase), and SBcl2 (radial growth phase) were provided by Dr. Meenhard Herlyn (Wistar Institute, Philadelphia, PA). Metastatic cell lines C8161 and MV3 were acquired from Fred Meyskens (University of California, Irvine Cancer Center) and Goos N.P. van Muijen (University Medical Center, Nijmegen, Netherlands), respectively. The M24met (metastatic) cell line was provided by Ralph Reisfeld (The Scripps Institute, San Diego, CA). Cell culture materials included Dulbecco's Modified Eagle's medium/Ham's F12 50:50 mix (DMEM/F12), RPMI-1640 medium, and Dulbecco's phosphate buffered saline (DPBS) and were purchased from Mediatech (Manassas, VA). Fetal bovine serum (FBS) was from GibcoBRL (Rockville, MD). Thrombin was obtained from Sigma (St. Louis, MO). RosetteSep Human NK cell enrichment cocktail and Ficoll-Paque PLUS were from Stemcell Tech (Tukwila, WA) GE Healthcare (Piscataway, NJ), respectively. Antibody labeling was done using anti-human CD-56 FITC conjugate from Invitrogen (Carlsbad, CA), and mouse IgG2a FITC, clone CBL601F, purchased from Cymbus Biotech (Hampshire,

UK). Antibodies for NKG2D ligands, Alexa Fluor 488 anti-human MICA/MICB (clone 6D4) were provided by Biolegend (San Diego, CA). Synthetic RGDS peptide was provided by ABBIOTECH (San Diego, CA). Atomic force microscopy tips were pyrex-nitride probe, triangular cantilevers obtained from Nano World Innovative Technologies (Neuchâtel, Switzerland) and silicon nitride tips from Bruker (Camarillo, CA). Hydrogen peroxide (30% w/w) was purchased from Sigma (St. Louis, MO), sulfuric acid (95-98% American Chemical Society grade reagent) from Sigma-Aldrich (St. Louis, MO), glutaraldehyde (25%, Electron Microscopy grade) and ethanol (absolute, 200 proof) from Electron Microscopy Science (Hatfield, PA). Human interleukin-2 (IL-2) was purchased from Pepro Tech, Inc. (Rocky Hill, NJ). FITC-labeled concanavalin A was obtained from EY laboratories Inc. (San Mateo, CA).

2.2. Cell Culture

All human melanoma cell lines were maintained in 100mm culture plates containing DMEM/F12 with 10% FBS at 37°C and 5% CO₂. For atomic force microscopy, cells were grown to 80-100% confluence, detached using 2mM EDTA, and transferred to a 60mm cell culture plate and incubated overnight in DMEM/F12 containing 10% FBS at 37°C and 5% CO₂.

2.3. Natural Killer Cell Isolation

Natural killer cells were isolated using the RosetteSep method. Briefly, whole blood was collected in sodium heparin (143 U.S. Pharmacopeia units), placed in a 50 mL conical tube, and 1000 µl of RosetteSep Human NK enrichment cocktail was

added. After mixing gently, the blood was incubated at room temperature (RT) for 20 minutes. The sample was diluted with an equal volume of PBS- 2% FBS that was equilibrated to RT and mixed gently. In two new 50 ml conical tubes, 20 ml of blood/PBS were layered on top of 15 mL RT Ficoll-Paque and centrifuged at 1200 g for 20 minutes at RT. After centrifugation, the top plasma layer was aspirated and NK cells from each conical tube were removed from the plasma/Ficoll-Paque interface. The NK cells from both tubes were combined, washed with an equal volume of PBS- 2% FBS and centrifuged at 300 g for 10 minutes. The NK cells were resuspended in five mL RPMI/10% FBS, stimulated with 750 IU/mL of IL2, and incubated at 37°C and 5% CO₂ until use. If the NK cells were not used within 48 hours of isolation they were restimulated with IL2 prior to use. For verification of the cell population, the NK cells were analyzed using an Accuri C6 flow cytometry (Ann Arbor, MI) via an anti-human CD56 FITC conjugated antibody against an IgG2a isotype control (see Section 2.8).

2.4. Preparation of recombinant eristostatin

The expression of recombinant eristostatin in *E. coli* was accomplished via a modification to a previously described method (Wierzbicka-Patynowski *et al.*, 1999). This method was modified using the pET 39b (+) expression plasmid and the use of the His*Bind column (Novagen, Madison, WI) for the isolation and thrombin-cleavage of the 6-histidine fusion protein. Eristostatin was finally purified using high performance liquid chromatography (HPLC) on an Agilent 1100 series system (Santa

Clara, CA) using a 5-60% gradient of acetonitrile in 0.02% trifluoroacetic acid (2 mL/min over 50 min).

2.5. Platelet aggregation

Eristostatin activity was confirmed by performing ADP-induced (20 μ M) platelet aggregation in a whole blood aggregometer from Chrono-Log Corp. (Havertown, PA). Human subject protocol approval was obtained by the University of Delaware Human Subjects Review Board in January 1998 and renewed in 2011 (154213-2). Aspirin-free blood was collected from healthy donors in 3.2% (w/v) sodium citrate (1:9 ratio). Aggregation inhibition was determined by subtracting the sample resistance value from the control resistance value, dividing by the control resistance value, and multiplying by 100 to give the percent inhibition. The percent inhibition and the concentration of the eristostatin were compared in Excel using a linear regression formula and the concentration of recombinant eristostatin that inhibited platelet aggregation by 50% (IC_{50}) was determined.

2.6. Atomic Force Microscopy

Silicon nitride probes with nominal spring constants of 0.01- 0.5 $N\ m^{-1}$ were cleaned with a piranha solution (30:70, H_2O_2 ; H_2SO_4) prior to functionalization. Surfaces of the AFM probes were silanized using a 4% solution of 3-aminopropyltrimethylethoxysilane in 95% ethanol for 1 hr at RT. Probes were washed in ethanol (>99.9%), dried for 5 min at 100°C, incubated for 10 min in 1.25% glutaraldehyde and washed in water. For blocking experiments, tips were incubated

overnight at 4°C in Er (0.1 mg/mL), and stored in PBS at 4°C until used. For NK experiments, tips were incubated with either concanavalin A (0.1 mg/mL) or anti-human CD56 FITC conjugated antibody (0.2 mg/mL) and brought into contact for five min with a culture of NK cells stimulated with IL2. Tips were withdrawn from the surface and an inverted light microscope was used to confirm the presence of a single NK cell. The plate of NK cells was removed and replaced by a plate of test cells for measurement of force curves. In some experiments, the melanoma cells were pre-incubated with 500 nM Er or 200 µM of a synthetic RGDS peptide for 30 minutes at RT before force curves were measured. Literature for use of RGDS peptides for adhesion studies suggests using a concentration in the mM range; however, it was observed with higher concentrations, that the cells no longer remained attached to the surface of the culture plate (Dehio *et al.*, 1998; McCarthy *et al.*, 1986). PicoForce contact mode was used for all measurements. Approximately 1000 forces curves were performed on 3 different cells. Of these, approximately 333 were performed at different areas on each cell, to make sure that the sampling was representative of the entire cell surface. To confirm repeatability, three separate AFM probes were used for each experimental condition. The distribution, average and standard error measurements were determined from these binding events.

2.7. Flow Cytometry

To test the purity of NK cells isolated using the RosetteSep method, 300 µL of the NK-RPMI/10% FBS mixture was transferred into 3 wells of a v-bottomed 96-well

plate. NK cells were spun for 30 seconds at 100 g and the supernatant decanted. Cells were washed (2x) in 100 μ L PBS-2% FBS with centrifugation for 30 seconds at 100 g. NK cells were resuspended in PBS-2% FBS and incubated for 10 minutes with PBS-2% FBS, IgG2a, and FITC labeled anti-human CD56 antibodies for unstained, isotype control, and CD56-stained treatments, respectively. The samples were strained into 5 mL BD falcon tubes for cytometric analysis.

For MICA/B surface expression assays, cell lines in DMEM/F12-10% FBS were incubated in the presence or absence of 3000 nM eristostatin for 1hr prior to beginning the protocol. Following aspiration of the media, cells were detached from the culture plate by incubating with 2mM EDTA for 5 minutes at 37° C. After resuspension in PBS- 2% FBS, the cells were transferred to a 15 mL conical tube and spun at 225 g for five minutes in 4° C. The supernatant was aspirated and the cells were resuspended in 5 mL PBS-2% FBS. A cell count was done using a hemacytometer and the cells were diluted or concentrated to a concentration of 1×10^6 cells/mL. A total volume of 200 μ L of the cell suspension (2×10^4 cells) was placed in wells of a v-bottom 96 well plate and 5 μ L of PBS-2% FBS, the isotype control, IgG2A, or anti-MICA/B antibodies were added. Cells were incubated for 30 minutes on ice in the dark. After incubation, the cells were spun for 40 seconds at 1400 g and washed (1x) with 200 μ L PBS-2% FBS. The samples were strained into 5 mL BD Falcon tubes and analyzed for MICA/B expression using an Accuri C6 flow cytometer.

For each cell line, treatments included unstained cells, the isotype control, and cells stained with Alexa fluor 488-anti-MICA/B antibody in triplicate.

2.8. Statistical Analysis

A Student's t-test was also applied to the data to determine the significant differences between the average unbinding forces detected. A p-value <0.05 was considered significant.

Chapter 3

RESULTS

3.1. Platelet Aggregation

The IC₅₀ value for each recombinant eristostatin was determined using whole blood platelet aggregation (Figure 3.1). The IC₅₀ values (mean ± SEM) for eristostatin (n=9) was 48.2 ± 14.5 nM. These values were similar to those previously reported (McLane *et al.*, 1994).

3.2. Direct unbinding of eristostatin and human melanoma cells

Atomic force microscopy was used to characterize the interactions via the unbinding forces between eristostatin and the surface of the melanoma cell lines. Eristostatin bound all six melanoma cell lines tested, C8161, MV3, M24met, 1205Lu, WM164, and SBcl2 with varying unbinding strengths (mean ± SEM) 0.38 ± 0.02 to 2.42 ± 0.03 nN (Figure 3.2). This interaction was partially inhibited with the addition of 500 nM soluble eristostatin in the media causing a significant decrease in the unbinding force from 1.54 ± 0.09 to 0.74 ± 0.14 nN (p = <0.0001), 2.42 ± 0.03 to 1.58 ± 0.05 nN (p = <0.0001), 0.38 ± 0.02 to 0.14 ± 0.02 nN (p = 0.039), and 0.76 ± 0.2 to 0.45 ± 0.3 nN (p = <0.0001) between eristostatin and C8161, MV3, M24met, and SBcl2 cell lines, respectively (mean ± SEM). 1205Lu and WM164, however,

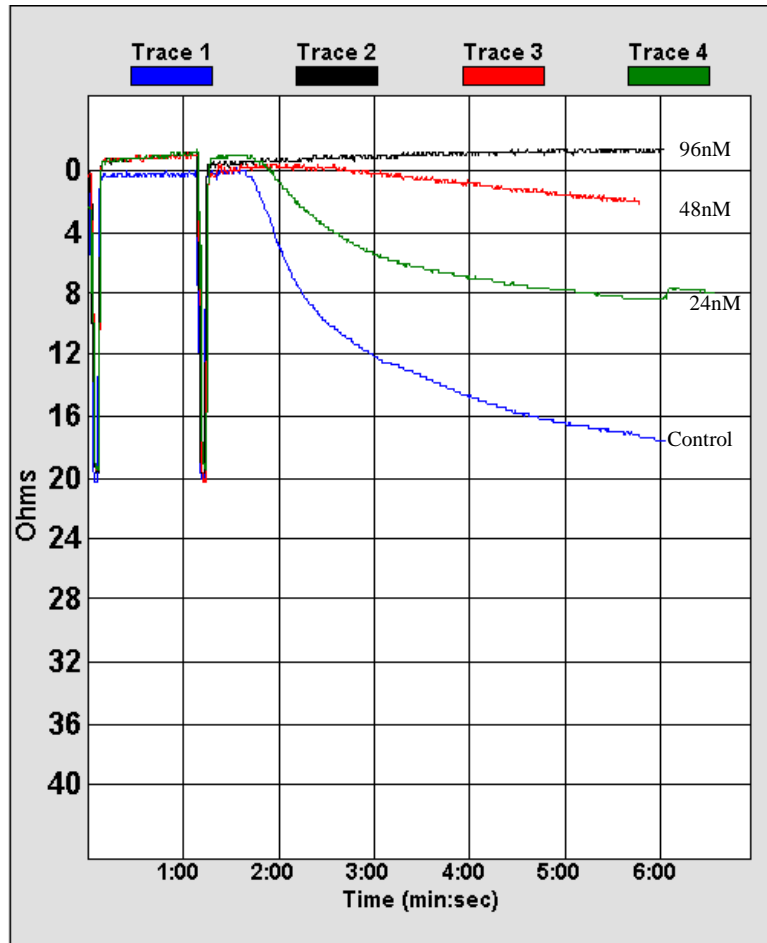


Figure 3.1. Representative platelet aggregation assay using eristostatin batch 7.2 208.081. Inhibition of ADP-induced whole blood platelet aggregation in the presence of eristostatin at 96 nM, 48 nM, and 24 nM dilutions compared to control.

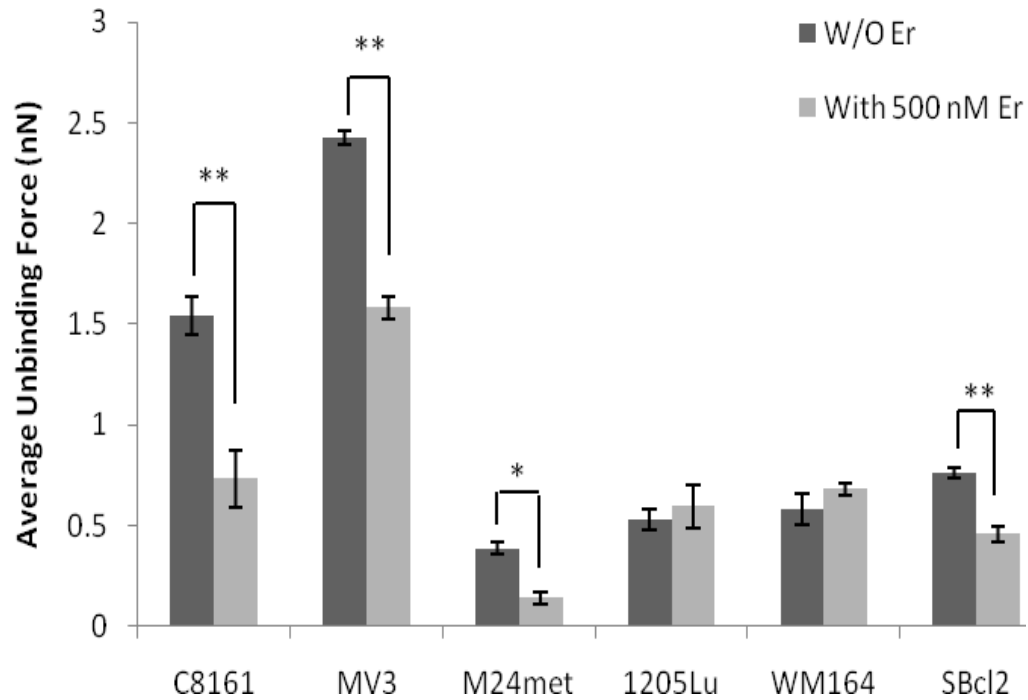


Figure 3.2. Average unbinding force between melanoma cells and eristostatin on the AFM cantilever tip. Eristostatin functionalized tips were brought into contact with indicated melanoma cell lines incubated for 30 min. in the presence or absence of 500 nM eristostatin. Data is mean unbinding force \pm SEM from at least three experiments; * $p = <0.05$; ** $p = <0.0001$; Er = eristostatin

did not show any significant changes in unbinding force after the addition of the soluble eristostatin (Figure 3.2). These two cell lines also did not show a decrease in the percent binding events compared to the total number of contacts after incubation with eristostatin (Table 3.1), while the other four cell lines did.

Table 3.1. Percentage of total contacts which showed unbinding events in the presence or absence of 500 nM eristostatin in solution with Er on the AFM tip.

| Melanoma Cell Line | % Unbinding Events | |
|--------------------|--------------------|-------|
| | -Er | +Er |
| C8161 | 17.56 | 12.62 |
| MV3 | 48.88 | 35.50 |
| M24met | 11.45 | 7.03 |
| 1205Lu | 10.38 | 21.03 |
| WM164 | 6.16 | 10.71 |
| SBcl2 | 59.74 | 26.83 |

Histograms of these interactions in the presence and absence of soluble eristostatin show trends which are not obvious in figure 3.2. For C8161, prior to the addition of eristostatin four major populations of unbinding events exist at 0.2 nN, 0.8 nN, 2.2 nN, and 4.1 nN. These unbinding events are shifted to 0.1 nN, 0.9 nN, and 2.4 nN, respectively, with the interaction population at 4.1 nN absent after soluble

eristostatin is added (Figure 3.3). MV3 melanoma cells exhibited four major peaks with a similar loss of the highest unbinding force population after eristostatin was added. The initial peak at the 0.2 nN unbinding force did not change. The remaining two populations increased from 1.0 nN to 2.2 nN and 2.9 nN to 3.2 nN (Figure 3.4). M24met showed only one unbinding population at 0.1 nN which remained the same after incubation with eristostatin (Figure 3.5). In the case of cell line, 1205Lu, there were three major populations. The initial population of unbinding events at 0.1 nN was unchanged in the presence of soluble eristostatin. The second and third peaks, however, were shifted towards lower strength forces: 0.6 nN to 0.4 nN and 1.3 nN to 0.9 nN (Figure 3.6). A histogram of the interactions between WM164 and eristostatin on the tip showed two groups of interactions at 0.1 nN and 0.9 nN. After the addition of eristostatin, the force of these interactions increased to 0.2 nN and 1.1 nN. In addition to these two groups of interactions changing, a new peak appeared at 1.4 nN (Figure 3.7). SBcl2 cells showed four peaks at 0.1 nN, 0.6 nN, 1.3 nN, and 1.7 nN of force. After eristostatin was added in solution, the first peak remained the same, the second peak increased to 0.7 nN and two peaks with the highest unbinding force were no longer present (Figure 3.8).

3.3. Partial inhibition of the eristostatin-melanoma cell interaction with RGDS peptide

To determine the possibility of an integrin binding partner, cells were incubated in the presence or absence of a synthetic RGDS peptide in AFM studies.

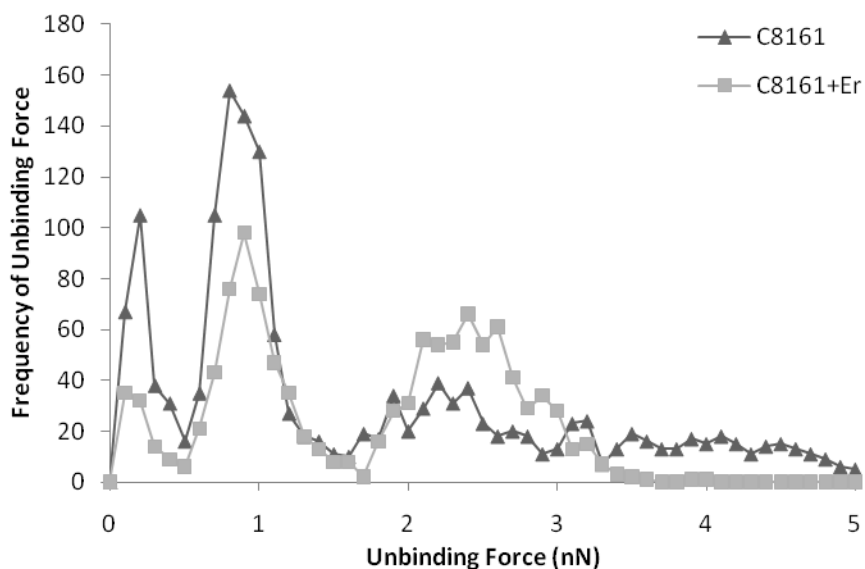


Figure 3.3. Frequency of unbinding events between C8161 and eristostatin functionalized AFM cantilever tips in the presence or absence of 500 nM eristostatin of at least 3 experiments.

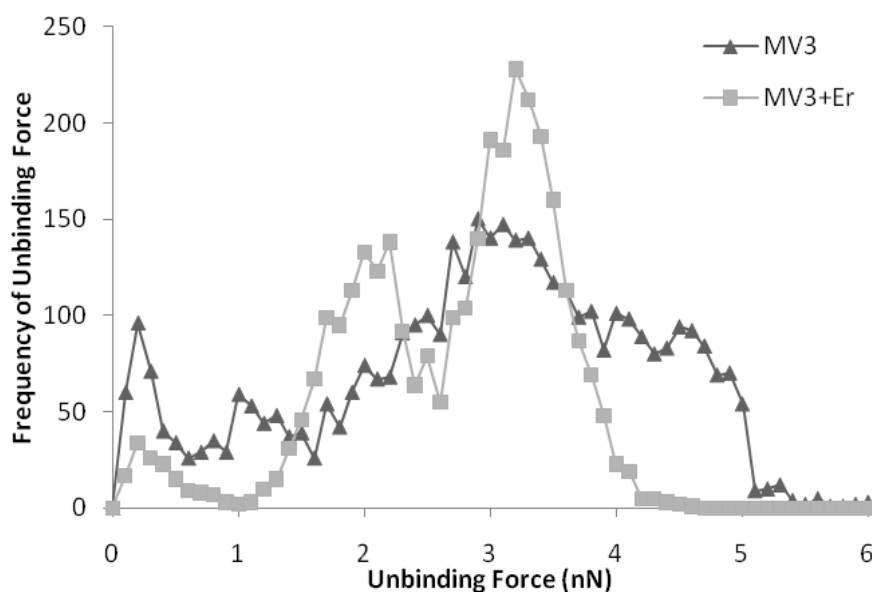


Figure 3.4. Frequency of unbinding events between MV3 and eristostatin functionalized AFM cantilever tips in the presence or absence of 500 nM eristostatin of at least 3 experiments.

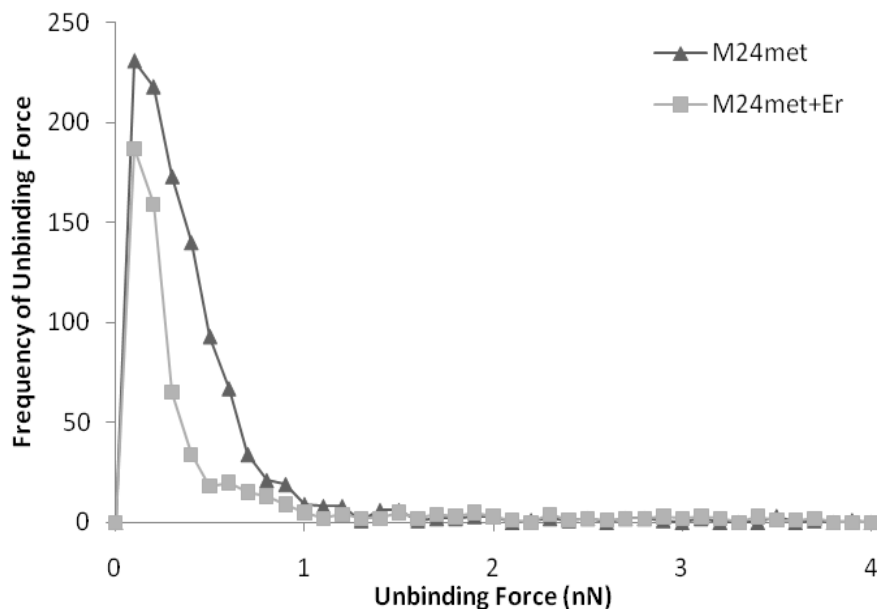


Figure 3.5. Frequency of unbinding events between M24met and eristostatin functionalized AFM cantilever tips in the presence or absence of 500 nM eristostatin of at least 3 experiments.

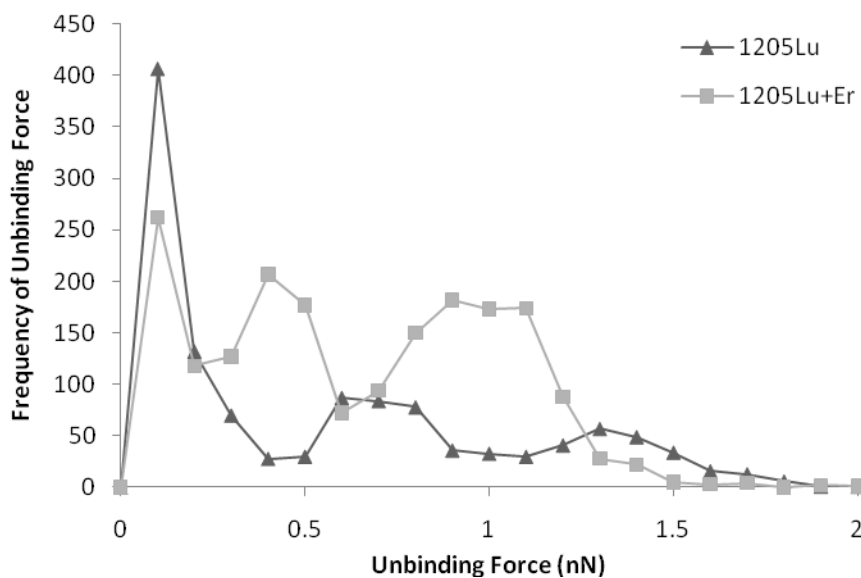


Figure 3.6. Frequency of unbinding events between 1205Lu and eristostatin functionalized AFM cantilever tips in the presence or absence of 500 nM eristostatin of at least 3 experiments.

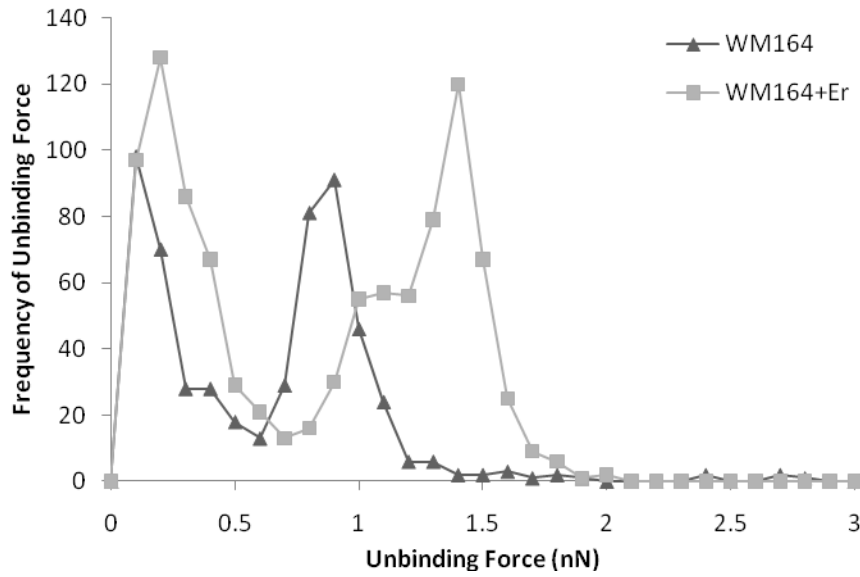


Figure 3.7. Frequency of unbinding events between WM164 and eristostatin functionalized AFM cantilever tips in the presence or absence of 500 nM eristostatin of at least 3 experiments.

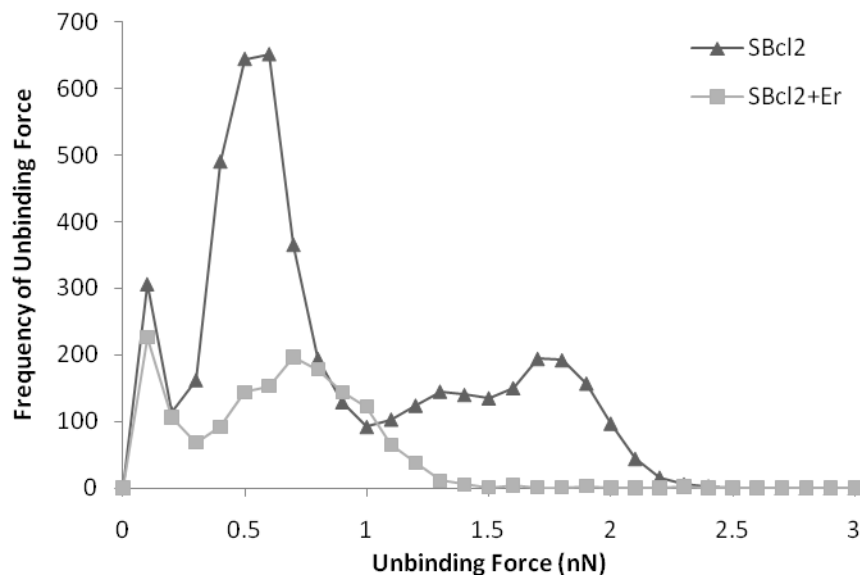


Figure 3.8. Frequency of unbinding events between SBcl2 and eristostatin functionalized AFM cantilever tips in the presence or absence of 500 nM eristostatin of at least 3 experiments.

All cell lines bound eristostatin and showed a decrease in the unbinding forces of eristostatin to their surface after the addition of the RGDS peptide. Of the six cell lines, only four cell lines showed inhibition which was significant. The unbinding forces for MV3, 1205Lu, WM164, and SBcl2 were significantly decreased by 0.78 nN ($p = <0.0001$), 0.27 nN ($p = <0.0001$), 0.27 nN ($p = 0.0318$), and 0.64 nN ($p = <0.0001$), respectively (Figure 3.9). Cell line C8161 appears to be significant, but after completing a Student's t-test, was not. Table 3.2 shows the change in the percentage of unbinding events after the addition of RGDS peptide in which C8161, MV3, 1205Lu, WM164, and SBcl2 experienced decreases. In contrast, M24met showed almost no change with a difference of 0.01% in the unbinding events compared to treatments in the absence of RGDS.

This data was also visualized using histograms. Interactions from eristostatin and C8161 yielded two major groups of unbinding events at 0.3 nN and 2.8 nN. RGDS peptide caused this to change to a single population of unbinding events at 0.5 nN (Figure 3.10). MV3 cells showed peaks at 0.3 nN, 0.7 nN, 1.7 nN, 2.2 nN, and 2.8 nN prior to the addition of RGDS which changed to 0.2 nN, 1.9 nN, and 2.2 nN after (Figure 3.11). For M24met cells, there was only one population of unbinding events for both treatments which was shifted from 0.3 nN to 0.1 nN in the absence and presence of linear RGDS peptide, respectively (Figure 3.12). 1205Lu showed one group of interactions at 2.4 nN in the absence of soluble RGDS.

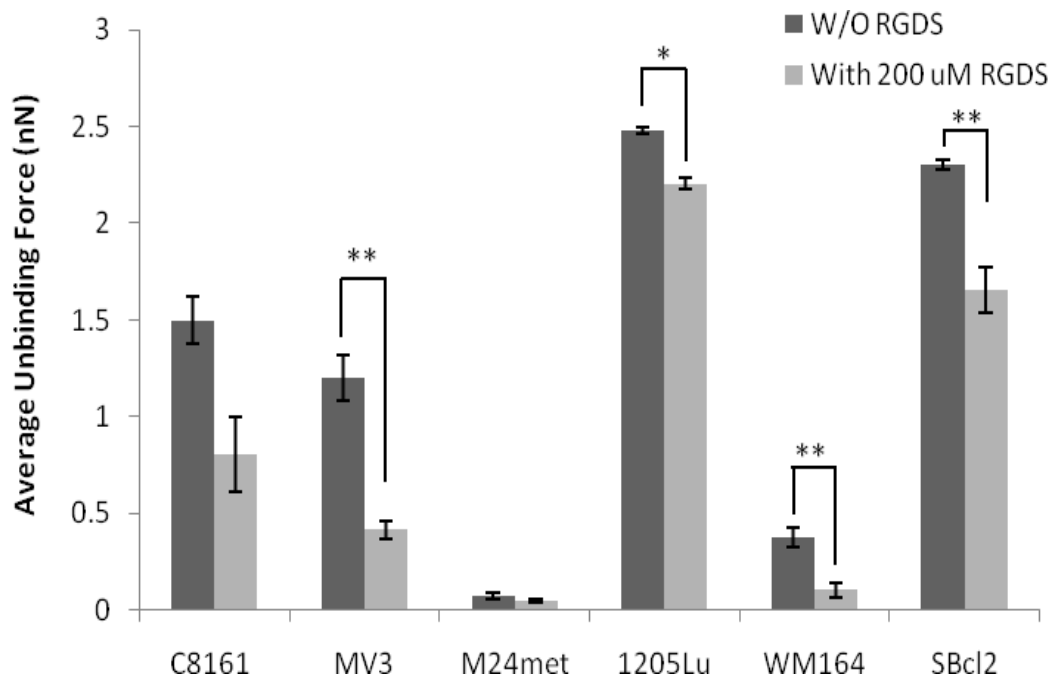


Figure 3.9. Average unbinding force between melanoma cells and eristostatin on the AFM cantilever tip. Eristostatin functionalized tips were brought into contact with indicated melanoma cell lines incubated for 30 min. in the presence or absence of 200 μ M synthetic RGDS peptide. Data is mean unbinding force \pm SEM from at least three experiments; * $p = <0.05$; ** $p = <0.0001$

Table 3.2. Percentage of total contacts which showed unbinding events in the presence or absence of 200 μ M RGDS in solution with Er on the AFM tip.

| Melanoma Cell Line | % Unbinding Events | |
|--------------------|--------------------|-------|
| | -RGDS | +RGDS |
| C8161 | 8.08 | 0.36 |
| MV3 | 5.03 | 2.21 |
| M24met | 1.01 | 1.02 |
| 1205Lu | 99.65 | 74.60 |
| WM164 | 3.85 | 0.80 |
| SBcl2 | 71.18 | 25.37 |

After incubation with RGDS, a new peak was present at 0.4 nN and the peak that was previously observed has shifted to 2.1 nN (Figure 3.13). WM164 exhibited two populations at 0.2 nN and 0.7 nN which changed to a single population at 0.1 nN (Figure 3.14). Unbinding events were recorded at three major populations for SBcl2 cells in both treatments. However, after incubation with RGDS peptide the second two peaks shifted from 1.1 nN to 1.4 nN and from 4.4 nN to 3.5 nN. The initial group of unbinding interactions remained constant at 0.2 nN (Figure 3.15).

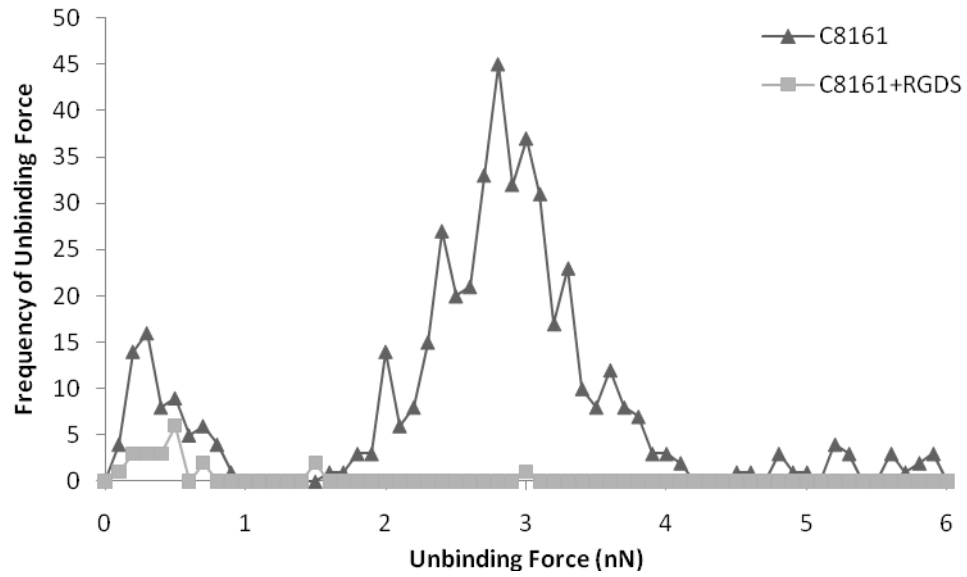


Figure 3.10. Frequency of unbinding events between C8161 and eristostatin functionalized AFM cantilever tips in the presence or absence of 200 μM RGDS peptide of at least 3 experiments.

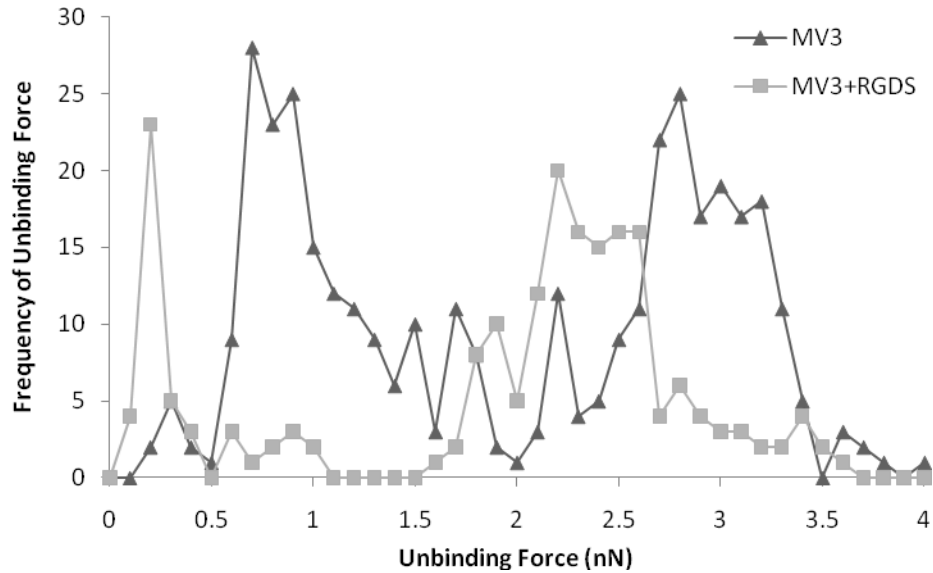


Figure 3.11. Frequency of unbinding events between MV3 and eristostatin functionalized AFM cantilever tips in the presence or absence of 200 μM RGDS peptide of at least 3 experiments.

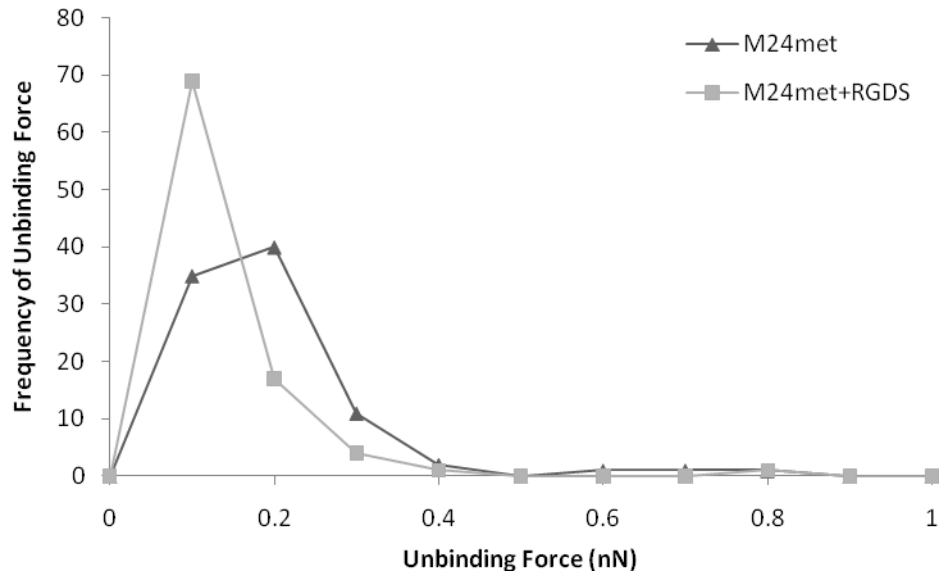


Figure 3.12. Frequency of unbinding events between M24met and eristostatin functionalized AFM cantilever tips in the presence or absence of 200 μ M RGDS peptide of at least 3 experiments.

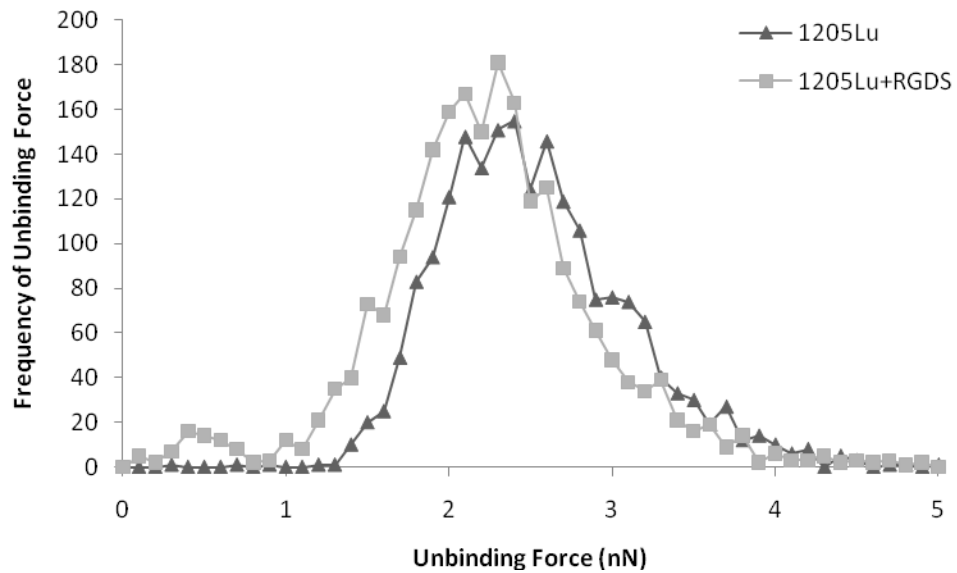


Figure 3.13. Frequency of unbinding events between 1205Lu and eristostatin functionalized AFM cantilever tips in the presence or absence of 200 μ M RGDS peptide of 1 experiment.

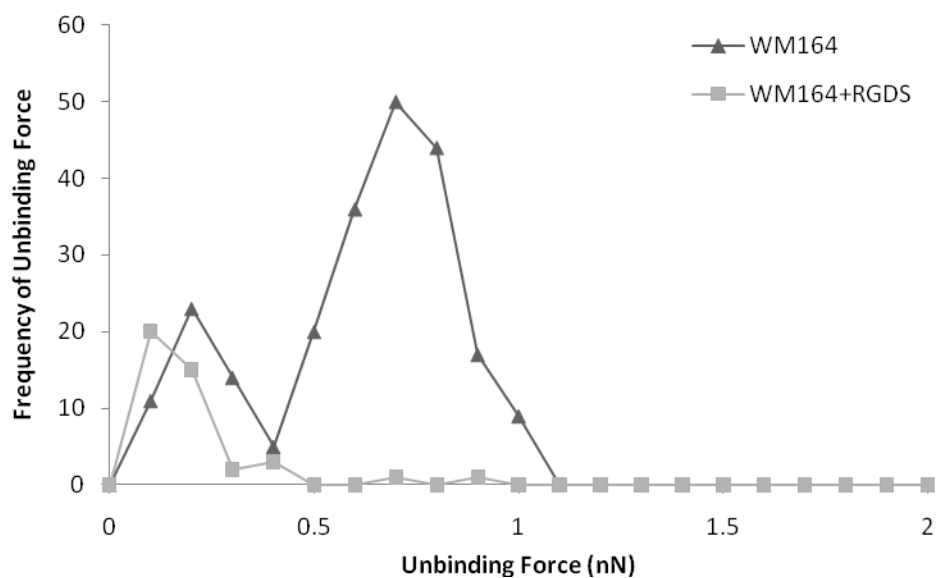


Figure 3.14. Frequency of unbinding events between WM164 and eristostatin functionalized AFM cantilever tips in the presence or absence of 200 μM RGDS peptide of at least 3 experiments.

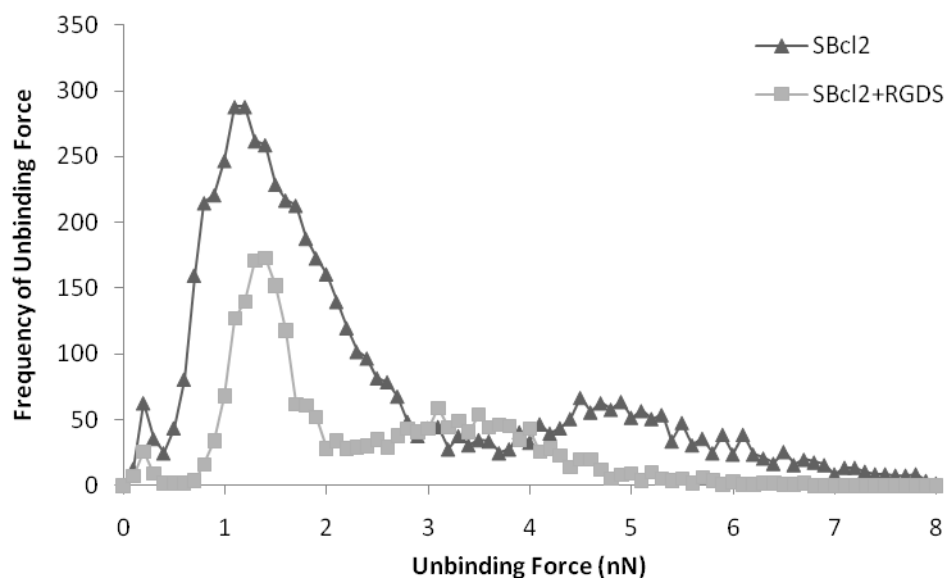


Figure 3.15. Frequency of unbinding events between SBcl2 and eristostatin functionalized AFM cantilever tips in the presence or absence of 200 μM RGDS peptide of at least 3 experiments.

It is important to note that during AFM experiments which occurred later in this project, approximately 70% of 1205Lu cells became detached from the surface of the plate after being left at room temperatures. No additional attempts to identify the cause of this phenomenon were completed.

A comparative table of unbinding populations among cell lines between eristostatin and RGDS AFM experiments summarizes the unique changes in unbinding events for each experimental condition (Table 3.3).

Table 3.3. Summary comparison of AFM unbinding populations between eristostatin functionalized tips and melanoma cells.

| Force Population (nN) | C8161 | MV3 | M24met | 1205Lu | WM164 | SBcl2 |
|-----------------------------|-------|-------|--------|--------|-------|-------|
| <0.3 | x/x/_ | x/x/x | x/x/x | x/x/_ | x/x/x | x/x/x |
| 0.4 | _/_- | _/_- | _/_- | _/x/x | _/_- | _/_- |
| 0.6 | _/_x | _/_- | _/_- | x/_/_ | _/_- | x/_/_ |
| 0.7 | _/_- | x/_/_ | _/_- | _/_- | x/_/_ | _/x/_ |
| 0.8 | x/x/_ | _/_- | _/_- | _/_- | _/_- | _/_- |
| 0.9 | _/_- | _/_- | _/_- | _/x/_ | x/_/_ | _/_- |
| 1.0 | _/_- | x/_/_ | _/_- | _/_- | _/_- | _/_- |
| 1.2 | _/_- | _/_- | _/_- | _/_- | _/_- | x/_/_ |
| 1.3 | _/_- | _/_- | _/_- | x/_/_ | _/_- | _/_- |
| 1.4 | _/_- | _/_- | _/_- | _/_- | _/x/_ | _/_x |
| 1.7 | _/_- | _/_- | _/_- | _/_- | _/_- | x/_/_ |
| 2.2 | x/_/_ | _/x/x | _/_- | _/_- | _/_- | _/_- |
| 2.3 | _/_- | _/_- | _/_- | _/_x | _/_- | _/_- |
| 2.4 | _/x/_ | _/_- | _/_- | x/_/_ | _/_- | _/_- |
| 2.8 | x/_/_ | x/_/_ | _/_- | _/_- | _/_- | _/_- |
| 2.9 | _/_- | x/_/_ | _/_- | _/_- | _/_- | _/_- |
| 3.1 | _/_- | _/_- | _/_- | _/_- | _/_- | _/_x |
| 3.2 | _/_- | _/x/_ | _/_- | _/_- | _/_- | _/_- |
| 4.1 | x/_/_ | _/_- | _/_- | _/_- | _/_- | _/_- |
| 4.5 | _/_- | x/_/_ | _/_- | _/_- | _/_- | x/_/_ |

X - Indicates presence of an unbinding population at the designated force for interactions between tip eristostatin and the melanoma cell under the following conditions; control/in the presence of soluble eristostatin/in the presence of soluble RGDS. Shading indicates interactions gained or lost in the presence of both 500 nM Er and 200 μM RGDS (light) or populations unique to eristostatin (dark).

3.4. Purity of freshly isolated natural killer cells

Natural killer cell populations isolated from freshly collected heparinized whole blood exhibited $\geq 90\%$ purity when analyzed by flow cytometry using anti-CD56 (Figure 3.16).

3.5. Direct unbinding of natural killer cell-melanoma cells

To determine any changes in the interactions between the melanoma cells and the natural killer cells due to eristostatin, direct force measurement assays using AFM were done in the presence and absence of 500 nM eristostatin. In the case of all six human melanoma cell lines, the natural killer cells, attached to the AFM cantilever tip (Figure 3.17), interacted with the surface of the melanoma cell. As shown in figure 3.18, the resulting interactions ranging from 0.14 ± 0.03 to 1.56 ± 0.15 nN of unbinding force (mean \pm SEM). Cell lines MV3 and WM164 showed a significant increase in the unbinding force between their surface and the natural killer cells from 0.54 ± 0.01 to 0.71 ± 0.02 nN ($p = <0.0001$) and 0.14 ± 0.03 to 0.35 ± 0.08 nN ($p = 0.0059$) respectively, whereas M24met displayed a significant decrease in its unbinding forces after the addition of eristostatin from 0.55 ± 0.05 nN to 0.39 ± 0.11 nN ($p = 0.009$) along with SBcl2 from 1.08 ± 0.01 nN to 1.01 ± 0.01 nN ($p = <0.0001$). C8161 and 1205Lu did not show any significant difference in the mean unbinding forces after the addition of eristostatin compared to the control (Figure 3.18).

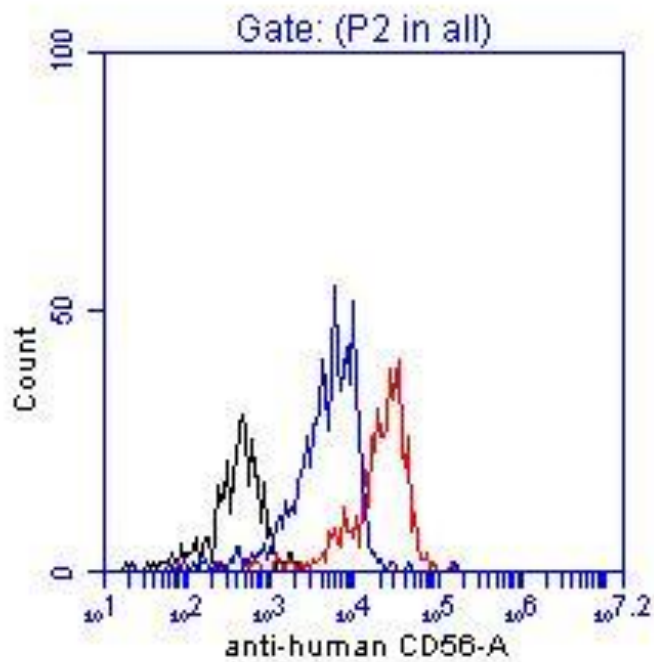


Figure 3.16. Representative flow cytometry histogram of freshly isolated natural killer cells. NK cells stained with anti-human CD56 antibody (red) showed greater than 90% purity compared to unstained (black) and isotype control (blue).

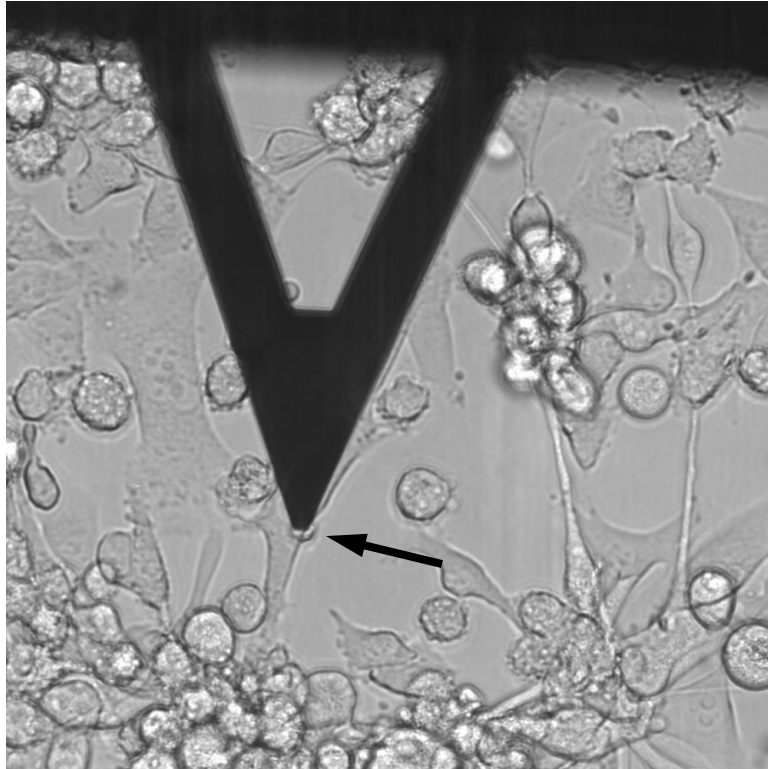


Figure 3.17. Natural killer cell (arrow) attached to tip of AFM cantilever tip engaged on WM164 human melanoma cell (200x).

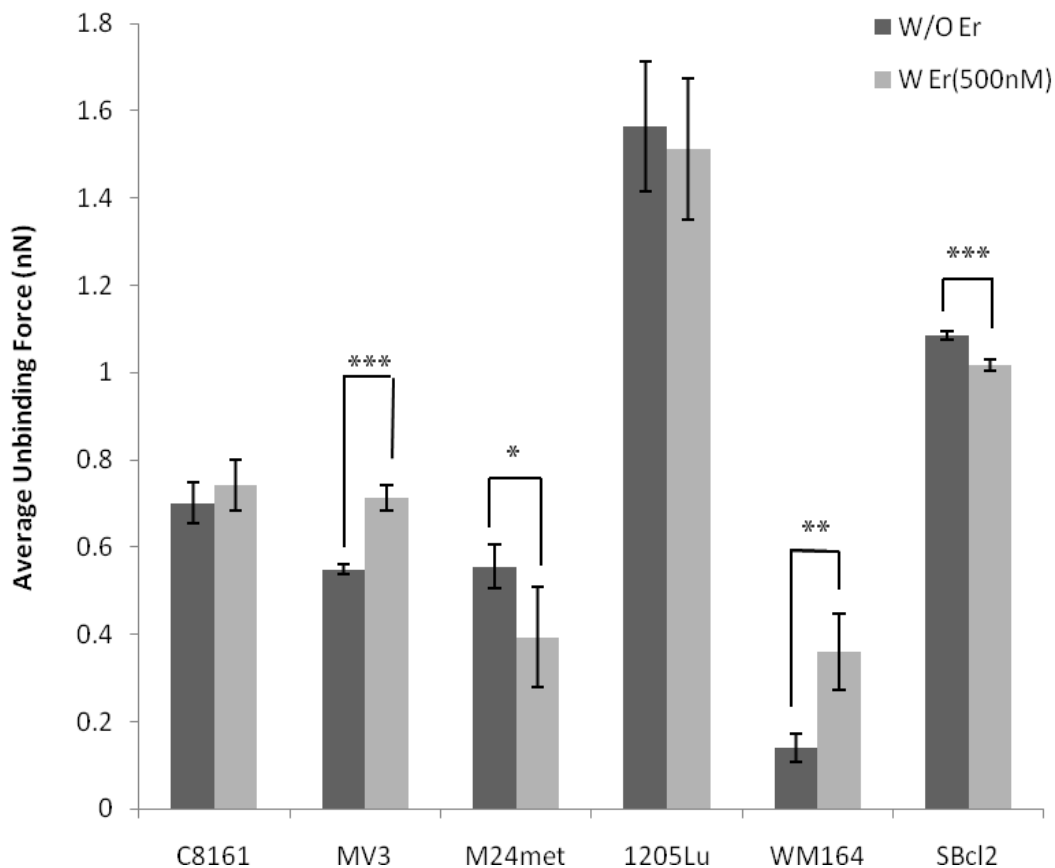


Figure 3.18. Average unbinding force between melanoma cells and natural killer cell on the AFM cantilever tip. NK cell functionalized tips were brought into contact with indicated melanoma cell lines incubated for 30 min. in the presence or absence of 500 nM eristostatine. Data is mean unbinding force \pm SEM from at least three experiments; * $p = <0.009$; ** $p = <0.0059$; * $p = <0.0001$**

Histograms of the unbinding forces which occurred between the natural killer cells and melanoma cells showed varying patterns in treatments with and without eristostatin. C8161 exhibited four major populations of interactions: approximately 0.1 nN, 0.4 nN, 1.1 nN, and 1.6 nN of force. After the addition of eristostatin, the three lower strength interactions were present; however, the population at the 1.6 nN range was no longer there (Figure 3.19). For MV3, there were initially four populations of unbinding events at 0.2, 0.6, 1.1, and 1.4 nN. These peaks, with the exception of the first at 0.2 nN, were shifted towards the higher force range to 0.8, 2.2 and 2.8 nN (Figure 3.20). M24met displayed only two major populations of events between the NK cells and its surface at 0.2 nN and 1.6 nN. With eristostatin, the events at 0.2 nN persisted; however, the population at 1.6 nN was no longer present and was replaced by a new peak at 0.6 nN (Figure 3.21). Direct force measurements for 1205Lu showed three major populations at 0.1, 2.8, and 8.3 nN. In contrast, eristostatin caused the loss of the interactions at the highest 8.3 nN range and emergence of a new population of unbinding events at 3.5 nN (Figure 3.22). WM164 cells showed low unbinding frequencies prior to the addition of eristostatin forming only two populations of interactions at 0.1 nN and 0.7 nN. Eristostatin caused an increase in the frequency at the 0.1 nN interaction and the loss of the second group of events at 0.7 nN (Figure 3.23). For SBcl2, there were two major interaction populations; however, the second peak was shifted from 1.7 nN to 1.6 nN in the presence of eristostatin (Figure 3.24).

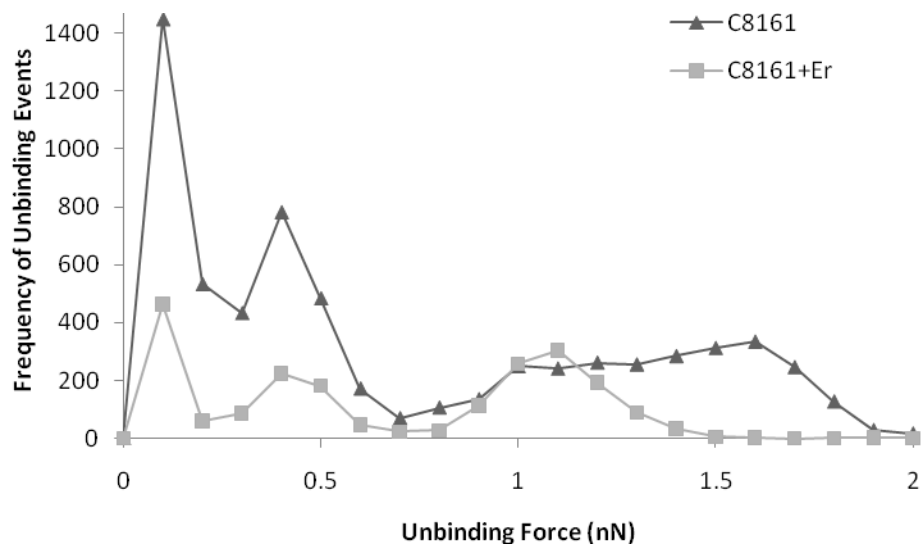


Figure 3.19. Frequency of unbinding events between C8161 and natural killer cell functionalized AFM cantilever tips in the presence or absence of 500 nM eristostatin of at least 3 experiments.

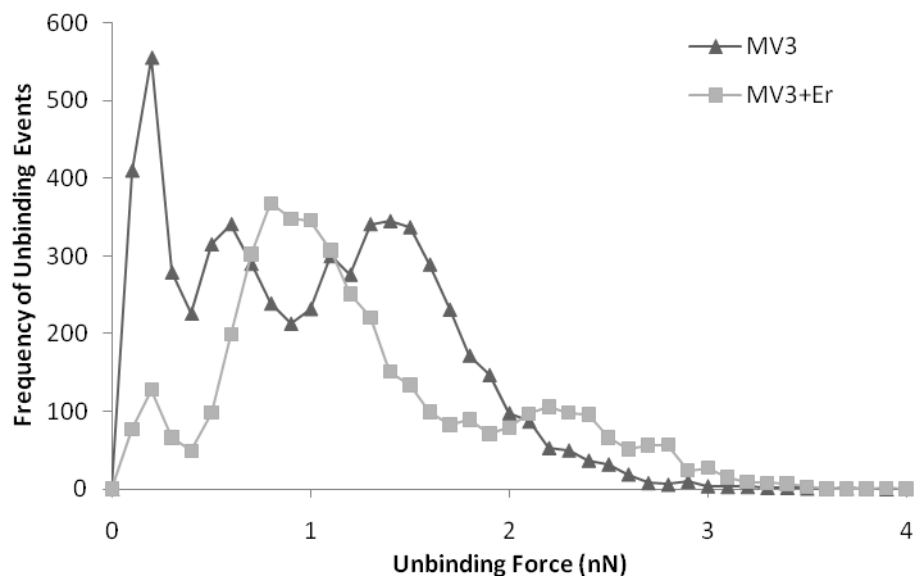


Figure 3.20. Frequency of unbinding events between MV3 and natural killer cell functionalized AFM cantilever tips in the presence or absence of 500 nM eristostatin of at least 3 experiments.

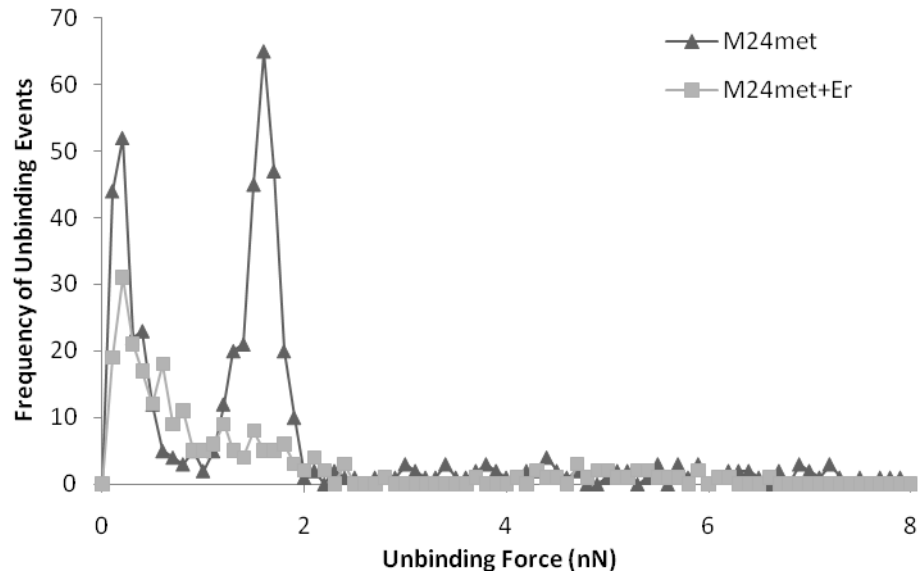


Figure 3.21. Frequency of unbinding events between M24met and natural killer cell functionalized AFM cantilever tips in the presence or absence of 500 nM eristostatin of at least 3 experiments.

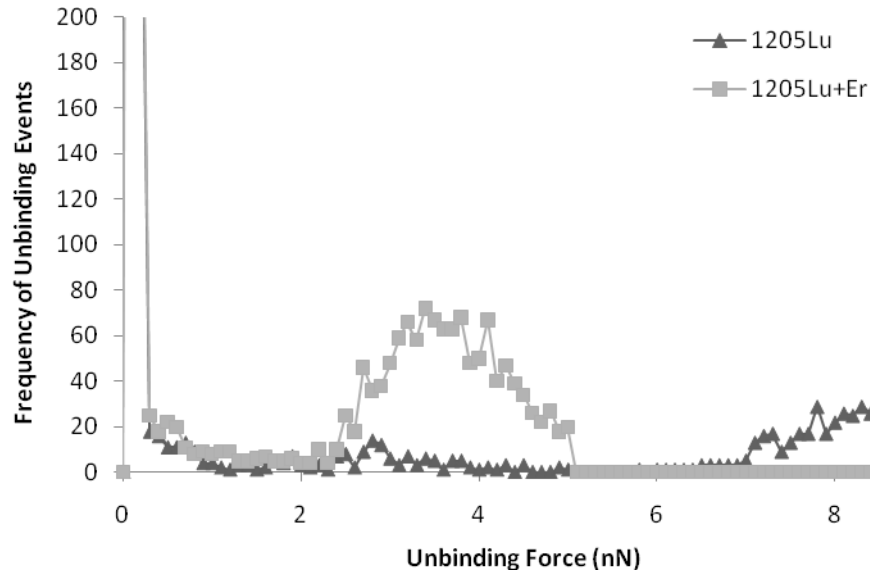


Figure 3.22. Frequency of unbinding events between 1205Lu and natural killer cell functionalized AFM cantilever tips in the presence or absence of 500 nM eristostatin of at least 3 experiments. (Note: initial peaks extends to above 500)

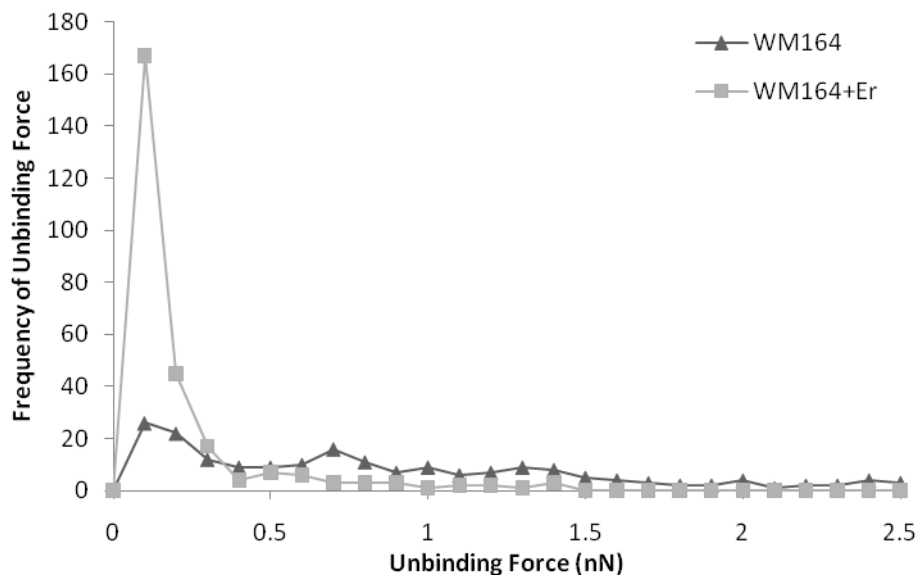


Figure 3.23. Frequency of unbinding events between WM164 and natural killer cell functionalized AFM cantilever tips in the presence or absence of 500 nM eristostatin of at least 3 experiments.

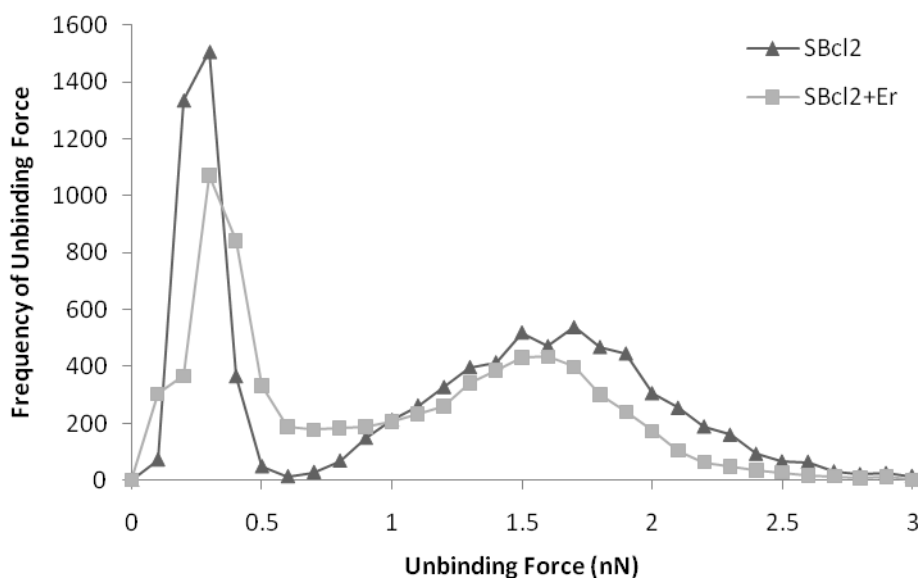


Figure 3.24. Frequency of unbinding events between C8161 and natural killer cell functionalized AFM cantilever tips in the presence or absence of 500 nM eristostatin of at least 3 experiments.

Comparisons of unbinding populations summarize differences and similarities between the unbinding of natural killer cells to each cell line in the presence and absence of soluble eristostatin (Table 3.4).

Table 3.4. Summary comparison of AFM unbinding populations between natural killer cell functionalized tips and melanoma cells.

| Force Population (nN) | C8161 | MV3 | M24met | 1205Lu | WM164 | SBcl2 |
|-----------------------|-------|-----|--------|--------|-------|-------|
| <0.3 | x/x | x/x | x/x | x/x | x/x | x/x |
| 0.4 | x/x | /- | /- | /- | /- | /- |
| 0.6 | /- | x/- | /- | /- | /- | /- |
| 0.7 | /- | /- | /- | /- | x/- | /- |
| 0.8 | /- | /x | /- | /- | /- | /- |
| 1.1 | /x | /- | /- | /- | /- | /- |
| 1.4 | /- | x/- | /- | /- | /- | /- |
| 1.6 | x/- | /- | x/- | /- | /- | /x |
| 1.7 | /- | /- | /- | /- | /- | x/- |
| 2.2 | /- | /x | /- | /- | /- | /- |
| 2.8 | /- | /- | /- | x/- | /- | /- |
| 3.4 | /- | /- | /- | /x | /- | /- |
| 8.3 | /- | /- | /- | x/- | /- | /- |

X - Indicates presences of and unbinding population at the designated force between natural killer cell and melanoma cells under the following conditions; control/in the presence of soluble eristostatin. Shading indicates the loss (light) or gain (dark) of populations in the presence of 500 nM Er.

3.6. Surface expression of NKG2D ligand, MICA/B

To determine the surface expression levels of the NKG2D ligand, MICA/B, flow cytometry was performed on all six cell lines. In addition to establishing basal expression levels, experiments were also run in order to identify any alterations as a result of incubation with 3000 nM eristostatin. For all six human melanoma cell lines, MICA/B was expressed on their surface. C8161 (Figure 3.25), MV3 (Figure 3.26), M24met (Figure 3.27), WM164 (Figure 3.28), and SBcl2 (Figure 3.29) did not show any change in fluorescence for treatments incubated with eristostatin. 1205Lu, however, showed a slight increase (19.9%) in fluorescence in cells incubated with 3000 nM eristostatin for 1 hour (Figure 3.30).

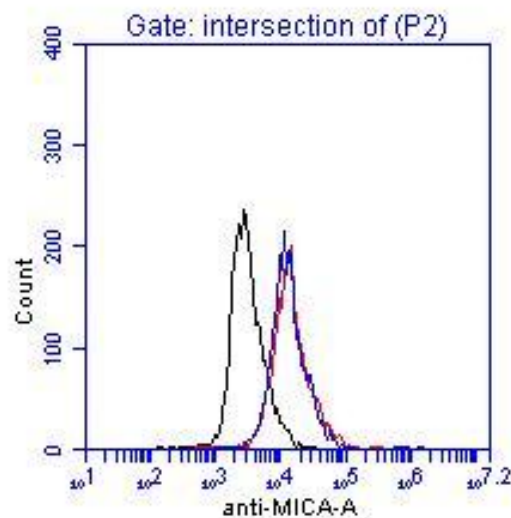


Figure 3.25. MICA/B expression on the surface of C8161 human melanoma cells. Expression of MICA/B assessed on cells incubated in the presence (blue) or absence (red) of eristostatin compared to unstained cells (black) from one experiment in triplicate.

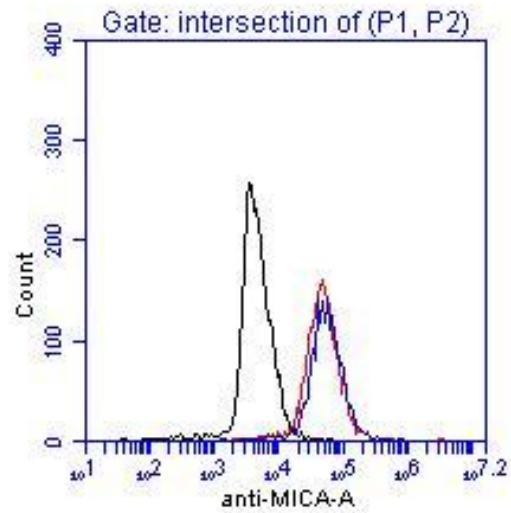


Figure 3.26. MICA/B expression on the surface of MV3 human melanoma cells. Expression of MICA/B assessed on cells incubated in the presence (blue) or absence (red) of eristostatin compared to unstained cells (black) from one experiment in triplicate.

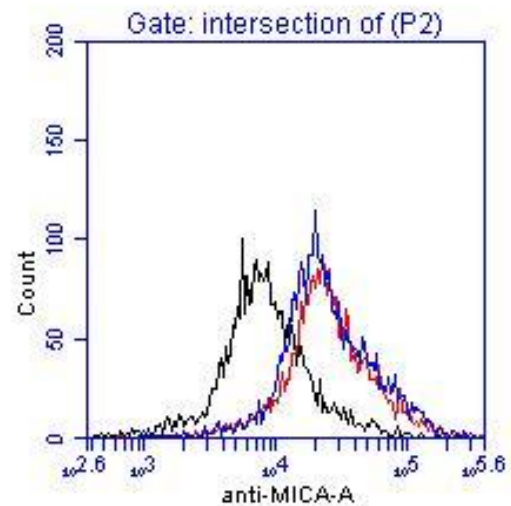


Figure 3.27. MICA/B expression on the surface of M24met human melanoma cells. Expression of MICA/B assessed on cells incubated in the presence (blue) or absence (red) eristostatin compared to unstained cells (black) from one experiment in triplicate.

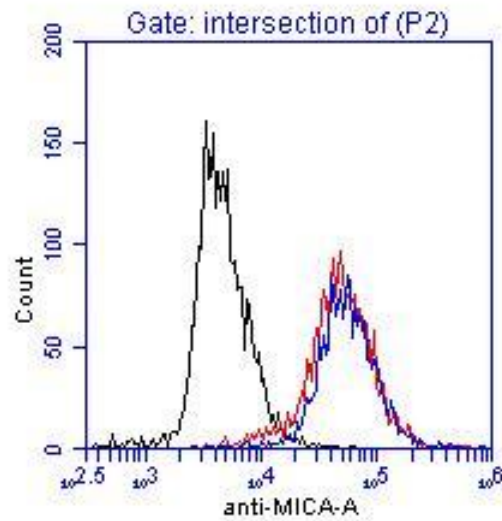


Figure 3.28. MICA/B expression on the surface of WM164 human melanoma cells. Expression of MICA/B assessed on cells incubated in the presence (blue) or absence (red) of eristostatatin compared to unstained cells (black) from one experiment in triplicate.

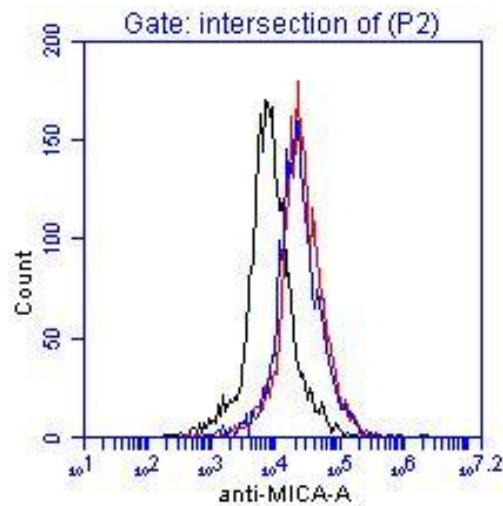


Figure 3.29. MICA/B expression on the surface of SBcl2 human melanoma cells. Expression of MICA/B assessed on cells incubated in the presence (blue) or absence (red) of eristostatatin compared to unstained cells (black) from one experiment in triplicate.

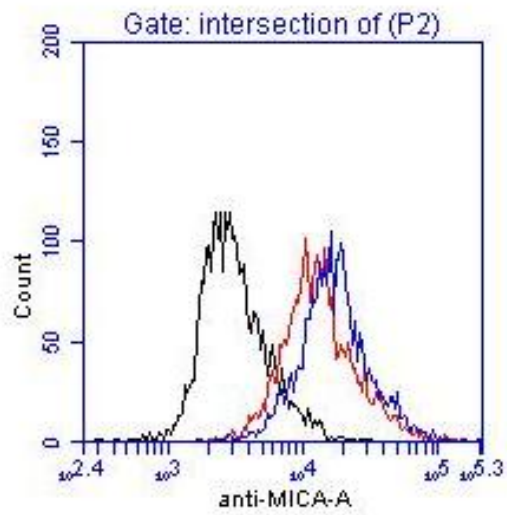


Figure 3.30. MICA/B expression on the surface of 1205Lu human melanoma cells. Expression of MICA/B assessed on cells incubated in the presence (blue) or absence (red) eristostatin compared to unstained cells (black) from one experiment in triplicate.

Chapter 4

DISCUSSION AND CONCLUSIONS

4.1. Discussion

Many disintegrins such as accutin (Yeh *et al.*, 1998), echistatin (Hallak *et al.*, 2005; Morte *et al.*, 2000), and contortrostatin (Markland *et al.*, 2001; Zhou *et al.*, 2000), have effective anti-cancer properties *in vitro* and/or *in vivo*. Often they exert their biological effect through antagonizing integrin binding, most commonly via $\alpha_v\beta_3$. This disruption can lead to inhibition of angiogenesis, induction of apoptosis, inhibition of metastasis, and inhibition of tumor regression (Yeh *et al.*, 1998; Hallak *et al.*, 2005; Morte *et al.*, 2000; Markland *et al.*, 2001; Oliva *et al.*, 2007).

Eristostatin also has properties which are anti-cancerous exemplified by the inhibition of lung and liver colonization, *in vivo*, of murine and human melanoma cells (Beviglia *et al.*, 1995; Morris *et al.*, 1995; Danen *et al.*, 1998; McLane *et al.*, 2003; Danen, 1995). The mechanism responsible for this effect, however, remains elusive.

One aim of this study was to determine the characteristics and possibly establish the molecule to which eristostatin is binding on the melanoma surface. AFM was used to measure direct unbinding forces and has proven to be a powerful tool in the quantification of forces between isolated proteins and/or intact mammalian cells (Benoit and Gaub, 2002; Lehenkari and Horton, 1999; Zhang *et al.*, 2004; Puech *et al.*, 2006). This study represents the first instance of testing direct disintegrin binding with

the use of AFM. All six human melanoma cell lines bound eristostatin to their surface as indicated by percent unbinding events of total contacts from 6-59% (Table 3.1) resulting in a range of unbinding forces from 0.38 nN to 2.42 nN (Figure 3.2). These results are higher than those observed by Lehenkari (1999) when measuring the direct unbinding forces between the disintegrin, echistatin, and osteoclasts (0.097 nN) through $\alpha_v\beta_3$ and between melanoma cells isolated from a vertical growth phase primary tumor, WM115, to fibronectin (0.5-0.75 nN) which contains an RGD motif and is largely dependent on β_1 integrins (Puech *et al.*, 2006).

Binding of eristostatin to four of the melanoma cells' surfaces also appears to be specific, having the properties of being reversible and saturable. This was demonstrated by the decrease in unbinding forces and percentage of unbinding events. However, these results did not show complete inhibition with the addition of soluble eristostatin in any of the melanoma cells tested. Additional evidence for this was observed in cell lines, 1205Lu and WM164, with no significant differences between treatments. Both of these phenomena (a partial and lack inhibition) may be due to dose dependence. Confocal data with cell lines such as 1205Lu corroborates this idea. Cells incubated with increasing concentrations of unlabeled eristostatin and stained with FITC-labeled eristostatin showed a reduced fluorescent signal only at the highest concentrations (1000 nM) of unlabelled eristostatin compared to controls (Figure 4.1). Therefore, higher concentrations of eristostatin may be needed in order to observe complete inhibition during AFM experiments. Testing with increasing concentrations of eristostatin would be ideal to answer this question but was not feasible for this project due to the quantity of eristostatin that would be needed for the numerous experiments that were done.

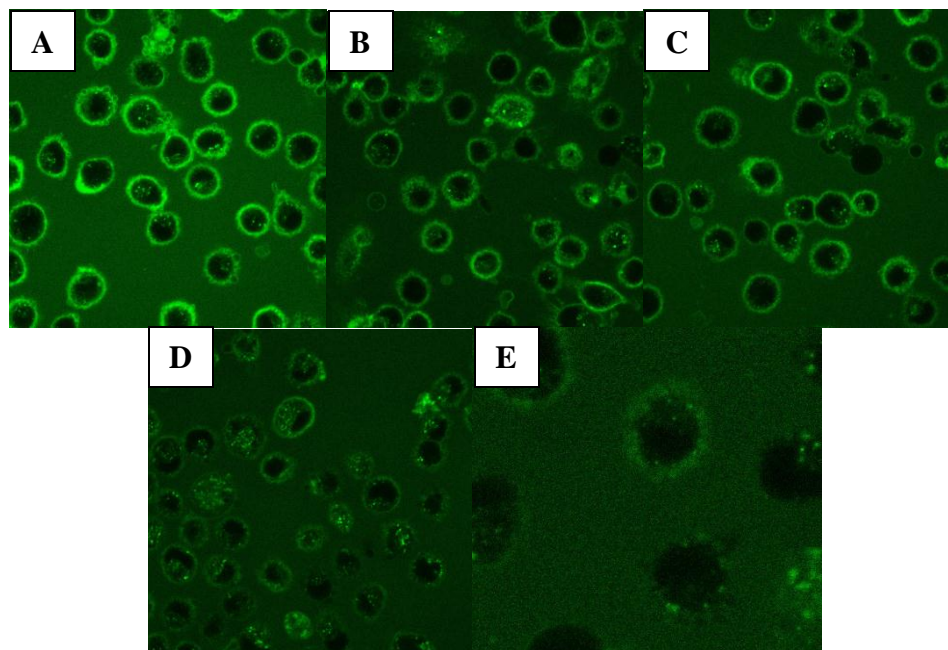


Figure 4.1. Confocal images of melanoma cell line 1205Lu stained with FITC-labeled eristostatin (A) in the presence of soluble eristostatin at 69 nM (B), 139 nM (C), 500 nM (D), and 1000 nM (E) concentrations. Photographs courtesy of Alice Wong, a previous member of Dr. McLane’s lab.

Histograms between eristostatin and all six melanoma cell lines revealed a common population of unbinding events in the range of 0.1 – 0.3 nN in both the presence and absence of eristostatin in solution. This population may be explained by intermolecular forces including electrostatic, ionic, and hydrophobic interactions present between the AFM probe and the melanoma surface (Aston and Berg, 2000; Kim *et al.*, 2008). This intermolecular force could also be due to interactions between molecules of eristostatin which are not presented in the proper orientation or by exposed glutaraldehyde amine group ends. The method of tip functionalization which

was employed in these experiments utilizes glutaraldehyde as binding agent which does not bind proteins in a consistent orientation. This results in a random percentage of bound eristostatin which may not be oriented in the correct position for normal receptor interaction (Berquand and Ohler, 2010).

A second commonality which existed among most of the cell lines is the presence of a population of unbinding interactions in the 0.4 – 1.0 nN range (Table 3.3). A prominent peak was not observed for M24met; however, binding did occur at that strength (Figure 3.5). This population may indicate that similar interactions are occurring between each of the melanoma cell lines comparable to measurements obtained by Puech et al. (2006) for the interaction between WM115 melanoma cells and fibronectin involving a β_1 integrin. The melanoma cell lines tested also exhibited groups of interactions at higher unbinding forces which appear to be in approximate multiples of lower forces (Figures 3.3-3.8). There are two ways to interpret this data. One explanation is that these data represent multiple unbinding interactions which occurred simultaneously and the summation of their unbinding strengths created an increase in affinity and thus an unbinding at higher force ranges. The AFM cantilever tip has a radius of 20 nm and eristostatin has a radius of approximately 1.1 nm (Erickson, 2009). This would allow multiple molecules of eristostatin to interact with the surface of the melanoma cell. A second explanation is that binding interactions are occurring between different receptors or surface molecules which unbind with various forces.

In addition to similarities among the cell lines in eristostatin binding characteristics, three changes occurred repeatedly to the unbinding events after the presence of soluble eristostatin as a blocking agent: (1) the frequency of the unbinding forces at lower unbinding strengths (< 1.0 nN) decreased (ex. Figure 3.3), (2) unbinding populations greater than 0.3 nN appeared to shift toward higher or lower strengths (ex. Figure 3.6), (3) individual unbinding populations were no longer present (ex. Figure 3.8). For this data, it cannot be determined if the observed shifts in the unbinding populations represent the same interactions at different force range or independent interactions; however, these most likely represent a change in the specific interactions that are occurring and not a shift in the strength of an unbinding event which has already occurred. Furthermore, it is possible that this observation may be due to the inhibition of one type of interaction by eristostatin which may then increase the prevalence or availability of a second type of interaction causing differences in unbinding force. We cannot at this time determine what physical changes in binding interactions result in the differences in unbinding characteristics identified in this data. It can, however, be hypothesized that the peaks at lower forces are subject to competition between soluble and tip eristostatin, whereas, unbinding populations at higher forces, which may be the result of different combinations of eristostatin-cell surface interactions, are more susceptible to conformational differences induced by soluble eristostatin. No trends or differences were observed between metastatic

(C8161, MV3, M24met, and 1205Lu), vertical growth phase (WM164), and radial growth phase (SBcl2) cell lines.

Previous efforts to determine a binding partner for eristostatin have implicated two integrins, $\alpha_{IIb}\beta_3$ (McLane *et al.*, 1994) and $\alpha_4\beta_1$ (Danen *et al.*, 1998). These integrins, however, are not expressed on the surface of all melanoma cell lines and thus seem to be poor candidates as a common receptor (Table 4.1). AFM data using RGDS peptide as an indicator of integrin-dependence showed that only partial inhibition is reached with the addition of RGDS to the media (Figure 3.9) which suggests two possible explanations. This partial inhibition could be due to concentration dependence as mentioned previously. Adhesion and motility studies

Table 4.1. Integrin surface expression repertoire on six human melanoma cell lines using flow cytometry versus literature.

| Integrin Subunit | Cell Line | | | | | |
|-------------------|-----------|-----|--------|--------|-------|-------|
| | C8161 | MV3 | M24met | 1205Lu | WM164 | SBcl2 |
| α_2 | +/+ | +/+ | +/ | +/+ | +/+ | /+ |
| α_5 | +/+ | +/- | -/- | -/- | +/- | /+ |
| α_{IIb} | -/- | -/- | -/- | -/- | -/- | /- |
| β_1 | +/+ | +/+ | +/+ | +/+ | +/+ | /+ |
| β_3 | +/+ | -/- | -/+ | +/+ | +/+ | /- |
| $\alpha_v\beta_3$ | -/+ | -/- | -/+ | +/+ | +/+ | /- |

+ indicates expression of integrin subunit; - indicates no expression; literature/our experiments. Data generated by Ryan Penn and Alice Wong.

using metastatic melanoma cells showed 80% inhibition with concentrations of RGDS peptide in the mM range (McCarthy *et al.*, 1986). It has also been documented in the literature that RGD peptides may only temporarily inhibit integrin binding (Ylanne, 1990). The second possibility is that eristostatin may not bind solely through an RGD-dependent pathway in all cell lines.

Focusing on the frequency of unbinding forces may give a better idea of the interactions that are taking place. For cell lines C8161 (Figure 3.10), MV3 (Figure 3.11), M24met (Figure 3.12), WM164 (Figure 3.14), and SBcl2 (Figure 3.15), data from RGDS blocking experiments with eristostatin-functionalized tips showed consistent populations of unbinding events similar to experiments with eristostatin on the tip in the presence of soluble eristostatin (Figure 3.3-3.8). In contrast, 1205Lu (Figure 3.13) displayed different patterns of unbinding frequencies between its surface and eristostatin during experiments blocking with eristostatin versus RGDS. This may be the result of changes in integrin and cell surface receptor expression due to increased passage number which caused the cell's detachment from the plate at room temperature during later RGDS experiments as mentioned previously (See Section 3.3). Similar morphological and physiological effects have been documented due to decreased passage number tolerance (Briske-Anderson *et al.*, 1997). Because cells must be stationary on the surface to obtain accurate AFM measurements, data was only recorded from 1205Lu cells which remained attached and this may have produced bias towards one specific sub-population within the cells.

C8161 (Figure 3.10) and WM164 (Figure 3.14) showed only two unbinding interactions at low and higher ranges prior to incubation with RGDS. For both cell lines the populations at the stronger forces were not observed in the presence of RGDS. This suggests that these interactions were RGD-dependent and thus most likely involved an integrin. This confirms previous data from Tian et al. (2007) in which C8161 and WM164 adhesion to an RGD matrix was disrupted by eristostatin indicating this interaction was occurring through an RGD-dependent mechanism. Comparisons between RGDS treatments among the other four cell lines indicate that this may not be the case for them. M24met (Figure 3.12) and 1205Lu (Figure 3.13) showed only slight change of 0.1 nN in the unbinding pattern before and after treatment with RGDS. This was mimicked in SBcl2 (Figure 3.15) although with a greater shift in the unbinding pattern (4.5 nN to 3.5 nN). These cell lines may not be as susceptible to changes in binding interactions due to RGDS. MV3 cells (Figure 3.11) showed both decreases and increases in unbinding force frequencies at specific interaction strengths. This is consistent with data which suggests MV3 is not solely dependent on RGD binding (Tian *et al.*, 2007). These secondary unbinding interactions may also be representative of secondary sites outside the RGD motif which may not be interrupted by a linear RGD peptide (Takagi, 2004).

In cell culturing, cells must synthesize and deposit extracellular matrix components in order to adhere to the polystyrene surface. Cells maintain adhesion through focal adhesions to this ECM. Most integrins aggregate and function within

these focal adhesions (Burrige and Chrzanowska-Wodnicka, 1996). This would suggest that the majority of integrins on the melanoma surface would be spatially and functionally unable to interact with eristostatin which is being presented on the top surface of the cell. This may provide additional evidence for the lack of RGD-dependence in eristostatin binding. However, depending on the specific ECM components which are present, not all integrins may be localized to the bottom of the cell and may allow for integrin binding elsewhere. It may also be possible that binding of eristostatin may induce integrin clustering on the top of the cell (Giancotti and Ruoslahti, 1999).

Comparisons of the unbinding populations present at specific forces for each cell line show changes unique to eristostatin. In addition, alterations in interaction populations that are common for both eristostatin-blocking and RGDS-blocking experiments are present. Interaction populations at specific unbinding forces between eristostatin and the melanoma cell showed a loss or gain of a single population in the presence of both soluble eristostatin and RGDS (Table 3.3, light shading). This provides additional evidence that these interactions are RGD-dependent and likely are due to integrin binding. In addition to this data, several populations are present in eristostatin-blocking experiments but not in RGDS-blocking experiments which may represent those interactions which are unique to eristostatin which are not dependent on the RGD motif. For example, C8161 exhibits a population of interactions at 2.4 nN only in the presence of eristostatin but not RGDS and the opposite is true for SBcl2 at

3.1 nN (Table 3.3, dark shading). There were however, no major patterns between cell lines for specific populations.

In this case, the data presented in AFM experiments in which the forces of unbinding events observed between eristostatin and the melanoma surface in the absence of soluble eristostatin or linear RGDS were highly variable. This lack of homogeneity among cell lines may be inconsistent with the presence of a common integrin binding partner for eristostatin. However, this may not be the sole explanation for the variability in unbinding force populations. The binding of the RGD motif by RGD-dependent integrins occurs primarily through the β subunit with residues outside of this region providing more direct specificity through the α subunit (Humphries *et al.*, 2006; Takagi, 2004). Calvete *et al.* (1994) demonstrated binding in this way via cross-linking to isolated $\alpha_{\text{IIb}}\beta_3$ integrins using four disintegrins, albolabrin, bitistatin, echistatin, and eristostatin. All four disintegrins cross-linked only to the β_3 subunit. This supports the possibility that eristostatin may bind via a common β integrin subunit. Secondary residues in the structure of eristostatin, which are functionally important such as the C-terminus and regions flanking the RGD loop (Tian *et al.*, 2007), would then allow it to bind with various strengths to integrin heterodimers which contain different α subunits.

Previous studies suggested that natural killer cell cytotoxicity may be responsible for the inhibitory effect that eristostatin has on melanoma cell colonization *in vivo* and that eristostatin may modulate normal natural killer cell behavior (McLane

et al., 2001). We have already determined that eristostatin binds directly to the surface of six melanoma cell lines. Here we show that direct binding of eristostatin to the melanoma surface can cause alterations in natural killer cell – melanoma cell interactions. AFM studies using NK cell-functionalized tips reveal variable results in mean unbinding forces among cell lines. Unbinding forces for MV3 and WM164 increased, M24met and SBcl2 decreased, and C8161 and 1205Lu showed no significant difference in the presence of eristostatin (Figure 3.18).

This variation is echoed in frequency data. However, among all cell lines there exists an initial population in the force range of 0.1 – 0.3 nN which most likely represents intermolecular forces discussed previously. C8161 (Figure 3.19), MV3 (Figure 3.20), 1205Lu (Figure 3.22), and SBcl2 (Figure 3.24) cell lines showed changes in the interactions between the NK cell and the melanoma cell in the presence of eristostatin. This manifested as a change in the unbinding strength from higher toward lower interaction forces (C8161, 1205Lu, and SBcl2) or as an increase in the unbinding strengths as seen in MV3 unbinding populations. For M24met (Figure 3.21) and WM164 (Figure 3.23), we did not see this same variation in the strength of unbinding but instead they exhibited the loss of an interaction population. In comparing individual interaction populations among cell lines, each cell line both lost (light shading) and gained (dark shading) at least one unbinding population between the NK cell and the melanoma cell in the presence of soluble eristostatin with the exception of M24met which lost a population but did not gain one (Table 3.4). It

cannot be determined if the unbinding populations which arose in the presence of eristostatin are due to changes in surface molecule interactions (new interactions) or a result of alterations in the characteristics of interactions which had previously occurred.

These results may reflect the various changes in surface interactions between NK cells and melanoma cell due to the modulation of the presentation and density of surface molecule clustering (Mostafavi-Pour *et al.*, 2003). The possibility also exists that eristostatin exerts a secondary effect by directly binding to natural killer cells altering the interactions between the NK cells and melanoma cells. McLane *et al.* (2001) determined that NK-like TALL-104 cytotoxicity levels increased when the TALL-104 cells and melanoma cells were simultaneously treated with eristostatin in addition to the increase seen when only melanoma cells were treated. Natural killer cells can bind target cells through β_1 and β_2 integrins, including $\alpha_4\beta_1$ (RGD-dependent), which are selective towards multiple intercellular adhesion molecules (Figure 4.2) and are important for proper adhesion of NK cells to target cells (Chong *et al.*, 1994; Gismondi *et al.*, 2003; Somersalo *et al.*, 1995). In addition to adhesion, activation of $\alpha_4\beta_1$ signaling may also causes the transcription of cytokines, such as interleukin-8, via the mitogen-activated protein kinase pathway (Figure 4.2), which play a role in NK cytotoxicity (Mainiero *et al.*, 1998; Mainiero *et al.*, 2000; Chua *et al.*, 2004). Interestingly, $\alpha_4\beta_1$ was proposed by Danen *et al.* (1998) as a possible target for eristostatin binding to MV3 melanoma cells. A disintegrin interaction with

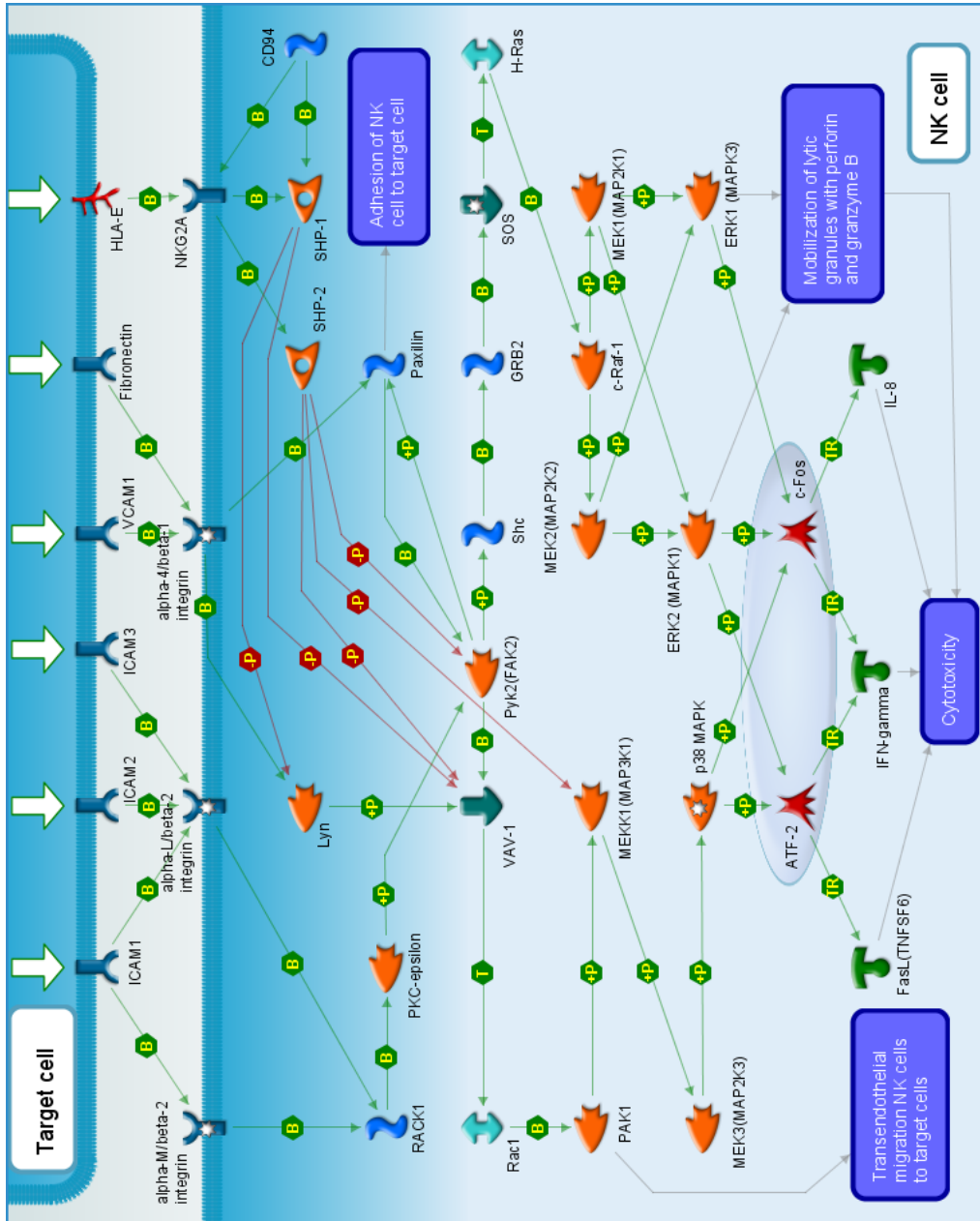


Figure 4.2. Natural killer cell integrin-mediated intracellular signaling and cytotoxicity (Genego, 2010).

leukocytes was described by Selistre-de-Araujo (2010) in which the disintegrin, jarastatin, induced several downstream integrin-mediated signaling events on neutrophils which expressed similar integrins, including β_1 , to lymphocytes (Selistre-de-Araujo *et al.*, 2010; Davenpeck *et al.*, 1998). Changes in adhesion may increase interactions between NK cells and targets cells necessary for activation and enhanced cytokine secretion would result in a rise in the immune response. These effects may be involved in eristostatin's ability to alter NK function and cytotoxicity.

Natural killer cell tumoricidal effects can be altered in the presence of platelets. Tumor cells both *in vivo* and *in vitro* were able to activate platelets which formed aggregates around the tumor cells, including B16F10 murine melanoma cells. This provided a novel mechanism for escape from NK-mediated cytotoxicity (Nieswandt *et al.*, 1999). The inhibition of the ability of the melanoma cells to form platelet aggregates thus preventing their disguise from NK cell detection, could be a potential mechanism from which eristostatin gains its effect *in vivo*. Beviglia *et al.* (1995) provided evidence for this effect demonstrating eristostatin's potency as an inhibitor of ADP and B16F10-induced platelet aggregation. However, it has also been documented that platelet aggregation is not necessary for cell arrest or extravasation to occur during hematogenous metastasis (Morris *et al.*, 1995). In addition, platelets were not present in the cytotoxicity studies reported by McLane *et al.* (2001), therefore, this does not seem to be a likely scenario in these current *in vitro* studies;

however, further investigation will be needed in determining an *in vivo* model of eristostatin's anti-metastatic effects.

In an effort to identify potential molecules responsible for the changes in NK cytotoxicity observed by McLane et al. (2001), the effect of eristostatin on surface expression of the NK activating receptor MICA/B was investigated using flow cytometry. Studies have suggested melanoma cells may develop the ability to retain MICA within their ER as a valuable protective agent against the immune system (Fuertes *et al.*, 2008). In contrast, all six melanoma cell lines tested exhibited surface expression of MICA/B (Figure 3.25-3.30), although variability existed between cell lines. In the presences of eristostatin, 1205Lu melanoma cells showed a 19.9 % increase in MICA/B expression. Cytotoxicity data (unpublished) for 1205Lu is consistent, showing significant increases in NK cell-mediated cytotoxicity with eristostatin treatment. MICA/B surface expression experiments were done with 1 hour exposure to eristostatin which may not be long enough to accurately detect the changes in surface expression due to transcriptional and post-translational regulation of MICA/B (Stern-Ginossar and Mandelboim, 2009). However, it is unlikely that this slight increase in expression was enough to alter NK function by itself due to the role of multiple NKG2D ligands and inhibitory receptors such as MHC-class I molecules (Zimmer, 2010; Stern-Ginossar and Mandelboim, 2009; Pende *et al.*, 2002). Cytotoxicity results using melanoma cell lines and fresh tissue from primary and metastatic tumors suggested that NK cytotoxicity is not directly correlated with surface

expression of MICA and that the ratio of NKG2D ligands to HLA class I expression plays an important role (Fuertes *et al.*, 2008). Future studies including natural killer cell inhibitory receptors, MHC-class I and other natural killer cell activating receptors such as UL-16 binding proteins 1, 2, and 3 (Zimmer, 2010) will be needed to more completely understand the effect of eristostatin on the melanoma-NK cell interaction.

4.2. Conclusion

In order to determine the effect of eristostatin on NK cell-melanoma cell interactions, we first confirmed that eristostatin bound the melanoma cell surface. AFM results established that binding did occur on all six melanoma cell lines tested. Similar interactions at 0.5-1.0 nN between all cell lines may point towards a common eristostatin binding partner, in particular a β_1 -containing integrin which is part of the integrin repertoire of each melanoma cell line. Interactions with higher unbinding forces > 0.5 nN were altered in the presence of soluble eristostatin and indicate that those populations are representative of eristostatin-melanoma surface binding. Studies using β_1 function-blocking antibodies or the utilization of siRNA to knock down the β_1 integrin subunit may be critical in determining eristostatin's binding partner.

Mean unbinding forces of eristostatin to melanoma cells also showed partial inhibition with linear RGDS peptide. C8161 and WM164 appeared to be RGD-dependent through the loss of their only major unbinding population in the presence of RGDS. The four remaining cell lines showed multiple interactions with eristostatin which were altered or remained similar with the addition of RGDS, suggesting a

binding mechanism not solely dependent on the RGD motif. Adhesion assays using eristostatin coated plates in the presence or absence of soluble RGDS peptide can be used to elucidate the RGD-dependence of each melanoma cell line.

Interactions between natural killer cells and melanoma cells in the presence of eristostatin showed substantial heterogeneity which affected both the frequency and force of unbinding. This result may point toward changes in surface molecule interactions (i.e. quantity and location) between NK cell and melanoma cells. In addition, the possibility of direct eristostatin-NK interactions exist which may affect natural killer cell function and cytotoxicity through downstream integrin-mediated signaling events. Further investigation in the role of melanoma cell-induced platelet aggregation may provide insight into the role of natural killer cells in the mechanism of eristostatin's action.

Finally, expression of MICA/B on the surface of six melanoma cell lines was assessed. Each cell line did express this NKG2D ligand on its surface and this expression was unaltered in the presence of eristostatin with the exception of 1205Lu. Eristostatin caused a slight increase in the surface expression of MICA/B on 1205Lu melanoma cells. However, this change may not be large enough to alter NK cell-mediated cytotoxicity and does not appear at this time to be part of a common mechanism among all six melanoma cell lines. A microarray or expression profile done over the course of multiple hours in the presence and absence of eristostatin would more likely show changes in expression on the surface of the melanoma cell.

Experiments to determine intracellular signaling events which occur as a result of eristostatin must be completed and will prove instrumental in identifying eristostatin's mechanism of action.

REFERENCES

- Altekruse, S. F., Kosary, C. L., Krapcho, M., Neyman, N., Aminou, R., Waldron, W., Ruhl, J., Howlander, N., Tatalovich, Z., Cho, H., Mariotto, A., Eisner, M. P., Lewis, D. R., Cronin, K., Chen, H. S., Feuer, E. J., Stinchcomb, D. G., and Edwards, B. K. (. (2009). SEER Cancer Statistics Review. **2010**.
- Aston, D. E. and Berg, J. C. (2000). Long-range attraction between silanated silica materials studied by an electrolyte titration with atomic force microscopy. *Colloids and Surfaces A: Physicochemical and Engineering Aspects*. **163**, 247-263.
- Benoit, M. and Gaub, H. E. (2002). Measuring Cell Adhesion Forces with the Atomic Force Microscope at the Molecular Level. *Cell Tissues Organs*. **172**, 174-189.
- Berquand, A. and Ohler, B. (2010). Common Approaches to Tip Functionalization for AFM-base Molecular Recognition Measurements. *Bruker Application Note*.
- Beviglia, L., Stewart, G. J., and Niewiarowski, S. (1995). Effect of Four Disintegrins of the Adgesive and Metastatic Properties of B16F10 Melanoma Cells in a Murine Model. *Oncology Research*. **7**, 7-20.

- Blanchard, C. R. (1996). Atomic Force Microscopy. *The Chemical Educator*. **1**, 1-8.
- Briske-Anderson, M. J., Finley, J. W., and Newman, S. M. (1997). The Influence of Culture Time and Passage Number on the Morphological and Physiological Development of Caco-2 Cells. *PSEBM*. **214**, 248-257.
- Burridge, K. and Chrzanowska-Wodnicka, M. (1996). Focal Adhesions, Contractility, and Signaling. *Annual Review of Cell Developmental Biology*. **12**, 463-519.
- Calvete, J. J., Marcinkiewicz, C., Monleon, D., Esteve, V., Celda, B., Juarez, P., and Sanz, L. (2005). Snake Venom Disintegrin: Evolution of Structure and Function. *Toxicon*. **45**, 1063-1074.
- Cesano, A. and Santoli, D. (1992). Two Unique Human Leukemic T-cell Lines Endowed with a Stable Cytotoxic Function and a Different Spectrum of Target Reactivity Analysis and Modulation of their Lytic Mechanism. *In Vitro Cell Dev Biol*. **28A**, 648-656.
- Chong, A. S., Boussy, I. A., Jiang, X. L., Lamas, M., and Graf, L. H. (1994). CD54/ICAM-1 is a Costimulator of NK Cell-mediated Cytotoxicity. *Journal of Cellular Immunology*. **157**, 92-105.
- Chua, H. L., Serov, Y., and Brahmi, Z. (2004). Regulation of FasL Expression in Natural Killer Cells. *Human Immunology*. **65**, 317-327.

- Danen, E. H. J. (1995). Cell Adhesion Receptors in Human Melanoma. In (Anonymous)pp 43-65.
- Danen, E. H. J., Marcinkiewicz, C., Cornelissen, I. M., Kraats, A. A., Pachter, J. A., Ruiter, D. J., Niewiarowski, S., and Muijen, G. N. P. (1998). The Disintegrin Eristostatin Interferes with Integrin $\alpha 4 \beta 1$ Function and with Experimental Metastasis of Human Melanoma Cells. *Experimental Cell Research*. 188-196.
- Davenpeck, K. L., Sterbinsky, S. A., and Bochner, B. S. (1998). Rat Neutrophils Express $\alpha 4$ and $\beta 1$ Integrins and Bind to Vascular Cell Adhesion Molecule-1 (VCAM-1) and Mucosal Addressin Cell Adhesion Molecule-1 (MAdCAM-1). *Blood*. **91**, 2341-2346.
- Dehio, M., Gomez-Duarte, O. G., Dehio, C., and Meyer, T. F. (1998). Vitronectin-dependent Invasion of Epithelial Cells by *Neisseria gonorrhoeae* Involves α -v Integrin Receptors. *FEBS Letters*. 84-88.
- Desgrosellier, J. S. and Cheresch, D. A. (2010). Integrins in cancer: biological implications and therapeutic opportunities. *Nature Reviews*. **10**, 9-22.
- Erickson, H. P. (2009). The Size and Shape of Protein Molecules at the Nanometer Level Determined by Sedimentation, Gel Filtration, and Electron Microscopy. **2011**.

- Fuertes, M. B., Girart, M. V., Molinero, L. L., Domaica, C. I., Rossi, L. E., Barrio, M. M., Mordoh, J., Rabinovich, G. A., and Zwirner, N. W. (2008). Intracellular Retention of the NKG2D Ligand MHC Class I Chain-related Gene A in Human Melanomas Confers Immune Privilege and Prevents NK Cell-mediated Cytotoxicity. *The Journal of Immunology*. **180**, 4606-4614.
- Giancotti, F. G. and Ruoslahti, E. (1999). Integrin Signaling. *Science*. **285**, 1028-1032.
- Gismondi, A., Jacobelli, J., Strippoli, R., Mainiero, F., Soriani, A., Cifaldi, L., Piccoli, M., Frati, L., and Santoni, A. (2003). Proline-rich Tyrosine Kinase 2 and Rac Activation by Chemokine and Integrin Receptors Controls NK Cell Transendothelial Migration. *Journal of Immunology*. **170**, 3065-3073.
- Gould, R. J., Polokoff, M. A., Friedman, P. A., Huang, T., Holt, J. C., Cook, J. J., and Niewiarowski, S. (1990). Disintegrins: A Family of Integrin Inhibitory Proteins from Viper Venom. *Proc Soc Exp Biol Med*. **195**, 168-171.
- Hallak, L. K., Merchan, J., Storgard, C. M., Loftus, J. C., and Russell, S. J. (2005). Targeted Measles Virus Vector Displaying Echistatin Infects Endothelial Cells Via alpha-v beta-3 and Leads to Tumor Regression. *Cancer Research*. **65**, 5292-5300.
- Han, W. and Serry, F. M. (2008). Force Spectroscopy with the Atomic Force Microscope. **2011**, 8.

- Herlyn, M., Clark, W. H., Rodeck, U., Mancianti, M. L., Jambrosic, J., and Koprowski, H. (1987). Biology of Tumor Progression in Human Melanocytes. *Lab Invest.* **56**, 461-474.
- Hsu, M., Meier, F., and Herlyn, M. (2002). Melanoma development and progression: a conspiracy between tumor and host. *Differentiation.* **70**, 522-536.
- Humphries, J. D., Byron, A., and Humphries, M. J. (2006). Integrin Ligands at a Glance. *Journal of Cell Science.* **119**, 3901-3903.
- Hynes, R. O. (2002). Integrins: Bidirectional, Allosteric Signaling Machines. *Cell.* **110**, 673-687.
- Kim, J. S., Jung, Y. J., Park, J. W., Shaller, A. D., Wan, W., and Li, A. D. Q. (2008). Mechanically Stretching Folded Nano-Pi-Stacks Reveals Pico-Newton Attractive Forces. *Advanced Materials.* **20**, 1-4.
- Lehenkari, P. P. and Horton, M. A. (1999). Single Integrin Molecule Adhesion Forces in Intact Cells Measured by Atomic Force Microscopy. *Biochemical and Biophysical Research Communications.* **259**, 645-650.
- Liddington, R. C. (2003). Structural Aspects of Integrins. In I Domains in Integrins (G. Donald, Ed.) Kluwer Academic/Plenum.
- Mainiero, F., Gismondi, A., Soriani, A., Cippitelli, M., Palmieri, G., Jacobelli, J., Piccoli, M., Frati, L., and Santoni, A. (1998). Integrin-mediated Ras-

Extracellular Regulated Kinase (ERK) Signaling Regulates Interferon gamma Production in Human Natural Killer Cells. *Journal of Experimental Medicine*. **188**, 1267-1275.

Mainiero, F., Soriani, A., Strippoli, R., Jacobelli, J., Gismondi, A., Piccoli, M., Frati, L., and Santoni, A. (2000). RAC1/P38 MAPK Signaling Pathway Controls b1 Integrin-Induced Interleukin-8 Production in Human Natural Killer Cells. *Immunity*. **12**, 7-16.

Markland, F. S., Shieha, K., Zhoua, Q., Golubkova, V., Sherwin, R. P., Richtersb, V., and Sposto, R. (2001). A Novel Snake Venom Disintegrin That Inhibits Human Ovarian Cancer Dissemination and Angiogenesis in an Orthotopic Nude Mouse Model. *Haemostasis*. **31**, 183-191.

McCarthy, J. B., Hagen, S. T., and Furcht, L. T. (1986). Human Fibronectin Contains Distinct Adhesion- and Motility-promoting Domains for Metastatic Melanoma Cells. *The Journal of Cell Biology*. **102**, 170-188.

McLane, M. A., Joerger, T., and Mahmoud, A. (2008). Disintegrins in Health and Disease. *Frontiers in Bioscience*. **13**, 6617-6637.

McLane, M. A., Kowalska, M. A., Silver, L., Shattil, S. J., and Niewiarowski, S. (1994). Interaction of Disintegrins with the $\alpha_{IIb}\beta_3$ receptor on resting and activated human platelets. *Biochem J*. 429-436.

- McLane, M. A., Kuchar, M. A., Brando, C., Santoli, D., Paquette-Straub, C. A., and Miele, M. E. (2001). New Insights on Disintegrin-Receptor Interactions: Eristostatin and Melanoma Cells. *Haemostasis*. 177-182.
- McLane, M. A., Marcinkiewicz, C., Vijay-Kumar, S., Wierzbicka-Patynowski, I., and Niewiarowski, S. (1998). Viper Venom Disintegrins and Related Molecules. *Proc Soc Exp Biol Med*. **219**, 109-119.
- McLane, M. A., Paquette-Straub, C. A., Wong, A., Srivastava, A., and Miele, M. E. (2003). Effect of the Disintegrin Eristostatin on Hematogenous Metastasis in Three Models of Human Malignant Melanoma. *Proc Amer Assoc Cancer Res*. 1180.
- McLane, M. A., Sanchez, E. E., Wong, A., Paquette-Straub, C., and Perez, J. C. (2004). Disintegrins. *Current Drug Targets- Cardiovascular & Haematological Disorders*. 327-355.
- Morris, V. L., Schmidt, E. E., Koop, S., MacDonald, I. C., Grattan, M., Khokha, R., McLane, M. A., Niewiarowski, S., Chambers, A. F., and Groom, A. C. (1995). Effects of the Disintegrin Eristostatin on the Individual Steps of Hematogeneous Metastasis. *Experimental Cell Research*. 571-578.
- Morte, R. D., Squillacioti, C., Garbi, C., Derkinderen, P., Belisario, M. A., Girault, J., Natale, P. D., Nitsch, L., and Staiano, N. (2000). Eristostatin inhibits pp125FAK

autophosphorylation, paxillin phosphorylation and pp125FAK-paxillin interaction in fibronectin-adherent melanoma cells. *FEBS Letters*. **267**, 5047-5054.

Mostafavi-Pour, Z., Askari, J. A., Parkinson, S. J., Parker, P. J., Ng, T. T. C., and Humphries, M. J. 1. (2003). Integrin Specific Signaling Pathways Controlling Focal Adhesion Formation and Cell Migration. *Journal of Cell Biology*. **161**, 155-167.

Nieswandt, B., Hafner, M., Echtenacher, B., and Mannel, D. N. (1999). Lysis of Tumor Cells by Natural Killer Cells in Mice is Impeded by Platelets. *Cancer Research*. **59**, 1295-1300.

O'Connor, R., Cesano, A., Lange, B., Fianan, J., Nowell, P. C., Clark, S. C., Raimondi, S. C., Rovera, G., and Santoli, D. (1991). Growth Factor Requirements of Childhood Acute T-Lymphoblastic Leukemia: Correlation Between Presence of Chromosomal Abnormalities and Ability to Grow Permanently In Vitro. *Blood*. **77**, 1534-1545.

Okuda, D., Koike, H., and Morita, T. (2002). A new gene structure of the disintegrin family: a subunit of dimeric disintegrin has a short coding region. *Biochemistry*. **41**, 14248-14254.

- Oliva, I. B., Coelho, R. M., Barcellos, G. G., Saldanha-Gama, R., Wermelinger, L. S., Marcinkeiwicz, C., Zingali, R. B., and Barja-Fidalgo, C. (2007). Effect of RGD-disintegrins on melanoma cell growth and metastasis: Involvement of the actin cytoskeleton, FAK and c-Fos. *Toxicon*. **50**, 1053-1063.
- Ouyang, C., Yeh, H., and Huang, T. (1983). A Potent Platelet Aggregation Inhibitor Purified from Agkistrodon Halys (Mamushi) Snake venom. *Toxicon*. **21**, 797-804.
- Pende, D., Rivera, P., Marcenaro, S., Chang, C., Biassoni, R., Conte, R., Kubin, M., Cosman, D., Ferrone, S., Moretta, L., and Moretta, A. (2002). Major Histocompatibility Complex Class I-related Chain A and UL16-Binding Protein expression on Tumor Cell Lines of Different Histotypes: Analysis of Tumor Susceptibility to NKG2D-dependent Natural Killer Cell Cytotoxicity. *Cancer Research*. **62**, 6178-6186.
- Plow, E. F., Haas, T. A., Zhang, L., Loftus, J., and Smith, J. W. (2000). Ligand Binding to Integrins. *The Journal of Biological Chemistry*. **275**, 21785-21788.
- Puech, P., Poole, K., Knebel, D., and Muller, D. J. (2006). A New Technical Approach to Quantify Cell-Cell Adhesion Forces by AFM. *Ultramicroscopy*. **106**, 637-644.

- Rigel, S. R., Russak, J., and Friedman, R. (2010). The Evolution of Melanoma Diagnosis: 25 Years Beyond ABCDs. *CA Cancer J Clin.* **60**, 301-316.
- Ruoslahti, E. and Pierschbacher, M. D. (1987). New Perspectives in Cell Adhesion: RGD and Integrins. *Science.* **238**, 491-497.
- Selistre-de-Araujo, P., C.L.S., Montenegro, C. F., and Martin, A. C. B. M. (2010). Snake Venom Disintegrins and Cell Migration. *Toxins.* 2606-2621.
- Somersalo, K., Carpen, O., Saksela, E., Gahmberg, C. G., Nortamo, P., and Timonen, T. (1995). Activation of Natural Killer Cell Migration by Leukocyte Integrin-Binding Peptide from Intracellular Adhesion Molecule-2 (ICAM-2). *Journal of Biological Chemistry.* **270**, 8629-8636.
- Stern-Ginossar, N. and Mandelboim, O. (2009). An integrated view of the regulation of NKG2D ligands. *Immunology.* **128**, 1-6.
- Takagi, J. (2004). Structural basis for ligand recognition by RGD (Arg-Gly-Asp)-dependent integrins. *Biochemical Society.* **32**, 403-406.
- Tian, J., Paquette-Strauba, C. A., Sageb, E. H., Funkb, S. E., Patelc, V., Galileo, D., and McLane, M. A. (2007). Inhibition of Melonoma Cell Motility by the Snake Venom Disintegrin Eristostatin. *Toxicon.* **49**, 899-908.
- Wierzbicka-Patynowski, I., Niewiarowski, S., Marcinkiewicz, C., Calvete, J. J., Marcinkiewicz, M. M., and McLane, M. A. (1999). Structural Requirements of

- Echistatin for the Recognition of $\alpha_v\beta_3$ and $\alpha_5\beta_1$ Integrins. *JBC*. **274**, 37809-37814.
- Yeh, C. H., Peng, H., and Huang, T. (1998). Accutin, a New Disintegrin, Inhibits Angiogenesis In Vitro and In Vivo by Acting as Integrin $\alpha_v\beta_3$ Antagonist and Inducing Apoptosis. *Blood*. **92**, 3268-3276.
- Ylanne, J. (1990). RGD peptides may only temporarily inhibit cell adhesion to fibronectin. *FEBS Letters*. **267**, 43-45.
- Zhang, X., Chen, A., Leon, D. D., Li, H., Noiri, E., Moy, V. t., and Goligorsky, M. S. (2004). Atomic Force Microscopy Measurement of Leukocyte-Endothelial Interactions. *Am J Physiol Heart Circ Physiol*. **286**, H359-H367.
- Zhou, Q., Sherwin, R. P., Parrish, C., Richters, V., Groshen, S. G., Tsao-Wei, D., and Markland, F. S. (2000). A Novel Snake Venom Disintegrin That Inhibits Human Ovarian Cancer Dissemination and Angiogenesis in an Orthotopic Nude Mouse Model. *Breast Cancer Research and Treatment*. **61**, 240-269.
- Zimmer, J., Ed. (2010). Natural Killer Cells: At the Forefront of Modern ImmunologySpringer, Heidelberg, Germany.

Appendix

PERMISSION LETTER



RESEARCH OFFICE

210 HULLIHEN HALL
UNIVERSITY OF DELAWARE
NEWARK, DELAWARE 19716-1551
Ph: 302/831-2136
Fax: 302/831-2828

DATE: January 4, 2011

TO: Mary Ann McLane, PhD
FROM: University of Delaware IRB

STUDY TITLE: [154213-2] Inhibition of Melanoma Metastasis by Eristostatin

SUBMISSION TYPE: Continuing Review/Progress Report

ACTION: APPROVED
APPROVAL DATE: January 4, 2011
EXPIRATION DATE: January 25, 2012
REVIEW TYPE: Expedited Review

REVIEW CATEGORY: Expedited review category # 2

Thank you for your submission of Continuing Review/Progress Report materials for this research study. The University of Delaware IRB has APPROVED your submission. This approval is based on an appropriate risk/benefit ratio and a study design wherein the risks have been minimized. All research must be conducted in accordance with this approved submission.

This submission has received Expedited Review based on the applicable federal regulation.

Please remember that informed consent is a process beginning with a description of the study and insurance of participant understanding followed by a signed consent form. Informed consent must continue throughout the study via a dialogue between the researcher and research participant. Federal regulations require each participant receive a copy of the signed consent document.

Please note that any revision to previously approved materials must be approved by this office prior to initiation. Please use the appropriate revision forms for this procedure.

All SERIOUS and UNEXPECTED adverse events must be reported to this office. Please use the appropriate adverse event forms for this procedure. All sponsor reporting requirements should also be followed.

Please report all NON-COMPLIANCE issues or COMPLAINTS regarding this study to this office.

Please note that all research records must be retained for a minimum of three years.

Based on the risks, this project requires Continuing Review by this office on an annual basis. Please use the appropriate renewal forms for this procedure.